Microcirculatory model predicts blood flow and autoregulation range in the human retina

Pappelis, Konstantinos; Choritz, Lars; Jansonius, Nomdo M.

Published in:
AMERICAN JOURNAL OF PHYSIOLOGY-HEART AND CIRCULATORY PHYSIOLOGY

DOI:
10.1152/ajpheart.00404.2020

Am J Physiol Heart Circ Physiol 319: H1253–H1273, 2020.
First published September 28, 2020; doi:10.1152/ajpheart.00404.2020.

RESEARCH ARTICLE | *Vascular Biology and Microcirculation*

Microcirculatory model predicts blood flow and autoregulation range in the human retina: in vivo investigation with laser speckle flowgraphy

Konstantinos Pappelis,[1,2] Lars Choritz,[3] and Nomdo M. Jansonius[1,2]

[1]*Department of Ophthalmology, University of Groningen, University Medical Center Groningen, Groningen, The Netherlands;* [2]*Research School of Behavioural and Cognitive Neurosciences, Graduate School of Medical Sciences, University of Groningen, Groningen, The Netherlands; and* [3]*University Eye Clinic, Otto von Guericke University Magdeburg, Magdeburg, Germany*

Submitted 29 May 2020; accepted in final form 16 September 2020

Pappelis K, Choritz L, Jansonius NM. Microcirculatory model predicts blood flow and autoregulation range in the human retina: in vivo investigation with laser speckle flowgraphy. *Am J Physiol Heart Circ Physiol* 319: H1253–H1273, 2020. First published September 28, 2020; doi:10.1152/ajpheart.00404.2020.—In this study, we mathematically predict retinal vascular resistance (RVR) and retinal blood flow (RBF), we test predictions using laser speckle flowgraphy (LSFG), we estimate the range of vascular autoregulation, and we examine the relationship of RBF with the retinal nerve fiber layer (RNFL) and ganglion cell complex (GCC). Fundus, optical coherence tomography (OCT), and OCT-angiography images, systolic/diastolic blood pressure (SBP/DBP), and intraocular pressure (IOP) measurements were obtained from 36 human subjects. We modeled two circulation markers (RVR and RBF) and estimated individualized lower/higher autoregulation limits (LARL/HARL), using retinal vessel calibers, fractal dimension, perfusion pressure, and population-based hematocrit values. Quantitative LSFG waveforms were extracted from vessels of the same eyes, before and during IOP elevation. LSFG metrics explained most variance in RVR ($R^2 = 0.77/P = 6.9{\cdot}10^{-9}$) and RBF ($R^2 = 0.65/P = 1.0{\cdot}10^{-6}$), suggesting that the markers strongly reflect blood flow physiology. Higher RBF was associated with thicker RNFL ($P = 4.0{\cdot}10^{-4}$) and GCC ($P = 0.003$), thus also verifying agreement with structural measurements. LARL was at SBP/DBP of 105/65 mmHg for the average subject without arterial hypertension and at 115/75 mmHg for the average hypertensive subject. Moreover, during IOP elevation, changes in RBF were more pronounced than changes in RVR. These observations physiologically imply that healthy subjects are already close to LARL, thus prone to hypoperfusion. In conclusion, we modeled two clinical markers and described a novel method to predict individualized autoregulation limits. These findings could improve understanding of retinal perfusion and pave the way for personalized intervention decisions, when treating patients with coexisting ophthalmic and cardiovascular pathologies.

NEW & NOTEWORTHY We describe and test a new approach to quantify retinal blood flow, based on standard clinical examinations and imaging techniques, linked together with a physiological model. We use these findings to generate individualized estimates of the autoregulation range. We provide evidence that healthy subjects are closer to the lower autoregulation limit than thought before. This suggests that some retinas are less prepared to withstand hypoperfusion, even after small intraocular pressure rises or blood pressure drops.

autoregulation; blood pressure; hemodynamics; mathematical modeling; retinal blood flow

INTRODUCTION

The retinal microcirculation is involved in many ophthalmic pathologies, but particular attention has been given to its role in leading causes of blindness, such as age-related macular degeneration, diabetic retinopathy, and glaucoma (74). In addition, it is often an indicator of cardiovascular or cerebrovascular disease (16a, 45). To date, there is only partial understanding of the regulation of blood supply in the retina and the optic nerve head (ONH), partially due to the lack of a gold-standard, noninvasive way to quantify blood flow (BF) (136).

The main advantage of the retinal vasculature is that it can be a direct source of physiological insight in humans, as a result of the transparent anterior ocular structures. However, there still are numerous caveats in assessing the retinal circulation. Despite its advantages, fluorescein angiography is an invasive procedure that only provides limited, qualitative information about tissue perfusion (66). With the development of optical coherence tomography angiography (OCTA), many additional characteristics of the retinal microvasculature can now be quantified noninvasively, but, when considered alone, they still do not describe BF in its entirety (62, 118). In addition, laser speckle flowgraphy (LSFG) is one among several promising techniques currently used for relative retinal BF dynamic evaluation (50, 124, 129). Details of this technique, as well as its application in the retina and the ONH, have been described elsewhere (28, 81, 124). In short, it calculates the mean blur rate (MBR) of the speckle pattern, which is caused by moving red blood cells and is roughly proportional to BF velocity. Its ability to quantify BF characteristics has already been demonstrated, but considerable technical limitations have to be overcome before LSFG can be introduced to the clinical setting (16, 82).

Consequently, there is no direct way to predict how individual microcirculatory determinants interact to determine tissue blood supply in the bigger picture. This interaction is complex: BF is driven by a pressure difference [ocular perfusion pressure (OPP)] but also depends on numerous properties of the vascular bed, such as autoregulation (AR). AR is the intrinsic ability of certain blood vessels to actively modify their caliber in response to changes in circumferential wall stress (110). Hence, the use of oversimplified perfusion surrogates such as OPP is a common shortcoming in ophthalmology. Indeed, not only does this approach run into serious statistical limitations in population studies, but it also disregards physiological compensatory mechanisms (67, 105).

In an attempt to complement the current assessment of retinal hemodynamics, current research mainly focuses on two

Correspondence: K. Pappelis (k.pappelis@rug.nl).

approaches. First, the emergence of Doppler OCT allows for absolute retinal blood flow quantification, which has been regarded as informative in describing physiological phenomena, as well as in detecting pathological changes (5, 76). Absolute retinal blood flow is a metric that partly addresses the limitations raised in the previous paragraph and is also the penultimate step in estimating tissue oxygenation (141). While the reproducibility of Doppler OCT is constantly being improved, it could still pose significant challenges in pathological conditions, since it requires considerably more expertise than standard imaging methods (127). Consequently, it has not found its way to the clinical routine yet. Second, mathematical models have been proposed, especially with regards to glaucoma, where a vascular component has long been thought to pertain to the disease pathogenesis (19, 34, 38, 43, 44, 83). However, these models have not attempted to describe quantitative BF metrics that could be easily obtained in everyday clinical care, hence immediately useful not only in physiological research, but also in diagnostic and treatment decisions. In addition, even though AR in the retina has been established as a general principle, each individual vasculature is unique. As such, it has distinct AR capacity that depends on its phenotype at a given point in time (extent of dilation/contraction, structural complexity, viscous forces, perfusion pressure, etc.). Neither approach is currently able to quantitatively predict the effect of blood pressure (BP) changes on BF physiology, considering these individual phenotypical characteristics.

Therefore, the primary aims of this study were *1*) to mathematically predict retinal vascular resistance (RVR) and absolute retinal blood flow (RBF), given individualized input collected with a proposed clinically feasible protocol, *2*) to test these predictions against in vivo BF measurements from human retinal vessels, and *3*) to provide individualized estimates for the range of retinal vascular AR. For this purpose, in the theoretical part of the study, we extended a model for the retinal microcirculation based on fractal geometry (128); in the experimental part, we examined the relationship of the theoretical predictions with BF information obtained from a human population in a clinical setting by means of LSFG. As a secondary aim, we looked into whether the model predictions for blood supply also reflect structural (nerve tissue) measurements.

METHODS

Study Population

The experimental part had a prospective, cross-sectional design. We included 36 eyes from 36 adult subjects. Participants underwent screening to exclude ocular pathologies. We did not exclude glaucoma, ocular hypertension, mild cataract (with best-corrected visual acuity $\geq$0.8), mild/moderate refractive error (−6D to +3D), and astigmatism of 2D or less. In order for the model to be tested over the full dynamic range of its variables, we encouraged participation of subjects with arterial hypertension (AHT), albeit no hypertensive retinopathy, and glaucoma. We used the standard AHT definition: current use of antihypertensive medication, or systolic blood pressure (SBP) $\geq$140 mmHg, or diastolic blood pressure (DBP) $\geq$90 mmHg (142). Glaucoma was defined as an already established clinical diagnosis, in accordance with the European Glaucoma Society guidelines (2). As a result, 15 of 36 subjects had AHT and 5 of 36 were patients from the ophthalmology clinic, already diagnosed with glaucoma [4 high-tension, primary open angle (POAG) cases, 1 primary closed angle case]. Eleven of 15 subjects with AHT were using antihypertensive medication, while all 5 glaucoma patients were using at least 1 topical antiglaucoma medication. The age of the participants ranged from 22 to 77 yr (median 54 yr).

Screening comprised a detailed slit lamp examination, best-corrected visual acuity (on a standardized letter chart), and C20–1 screening mode frequency doubling perimetry (Carl Zeiss, Jena, Germany). Additional documentation of ophthalmic health was performed with the imaging session (fundus photography, OCT, and OCTA; see METHODS, *Model Variables and Parameters*, *Central retinal artery and vein radii* and *Fractal dimension*). Apart from the glaucoma patients, all other participants had healthy eyes, while there were no subjects with diagnosed diabetes or cardiovascular disease (except for AHT). All tests were performed in the ophthalmology clinic, under similar conditions (room temperature 22.5–23.5°C), and with undilated pupils, since some mydriatic drops (alpha-adrenergic agonists) could affect certain BF metrics (81). Other studies have used muscarinic antagonists for pupil dilation, without any notable effect on BF (82).

The ethics board of the Otto von Guericke University Magdeburg approved the study protocol (No. 32/19). All participants received an information letter and provided written informed consent. The study followed the tenets of the Declaration of Helsinki.

Model Variables and Parameters

Central retinal artery and vein radii. We obtained 45° fundus photographs centered at the ONH in high resolution from all subjects with a nonmydriatic digital camera (nonmyd WX-3D, Kowa Company, Ltd., Japan). We used the revised Parr-Hubbard formulas proposed by Knudtson et al. and a freely available, semiautomatic software [Automated Retinal Image Analyzer (ARIA), Peter Bankhead] to derive the central retinal artery and vein equivalents (CRAE and CRVE) (8, 71). Details of this procedure have been described elsewhere (71). In short, a standardized number of six largest arteriolar and six largest venular branches were identified within a ring with borders at 0.5- and 1.0-optic-disk diameters from the ONH margin (Fig. 1*A*); subsequently, an iterative mathematical procedure, using the area expansion ratio of the daughter branches to the mother branch, returned the expected radii of the CRA and CRV (r_{a_0}, r_{v_0}).

Branch length exponent (α) and branch length coefficient (β). The microvascular bed can be decomposed into two distinct fractal patterns: one with regards to the exponential decay in branch radius r and one with regards to the decay in the corresponding branch length l, as the order i of the branches increases. Assuming symmetric, dichotomous branching (see METHODS, *Model Building*), we may write:

$$\begin{cases} r_i = r_0 e^{-i\tau} \\ l_i = l_0 e^{-i\sigma} \end{cases} \quad (1)$$

where i is an integer representing the branch order and τ and σ are rate parameters. It follows that:

$$l_i = \beta r_i^{\alpha} \quad (2)$$

$$\text{where } \beta = \frac{l_0}{r_0^{\alpha}} \text{ and } \alpha = \frac{\sigma}{\tau}.$$

For the branch length exponent α, we use the constant suggested by Takahashi et al. for the retinal vasculature, $\alpha = 1.15$, which is based on data from cerebral vessels (128). Regarding the branch length coefficient β, *Eq. 2* suggests that it is dependent on the stem radius; hence, its baseline value can be altered in conditions such as AHT or glaucoma (65, 69, 132). Takahashi et al. use the value $\beta = 7.4$, but this was calculated from an average of young, healthy individuals (128). Assuming vasodilation/vasoconstriction are length-preserving, collective, and uniform transformations of the vessels, we calculate the corrected branch length coefficients β_a and β_v from each individual CRA and CRV, based on their deviation from the average radii r_{a_0} and r_{v_0}, determined from the 18 healthy normotensives in our study:

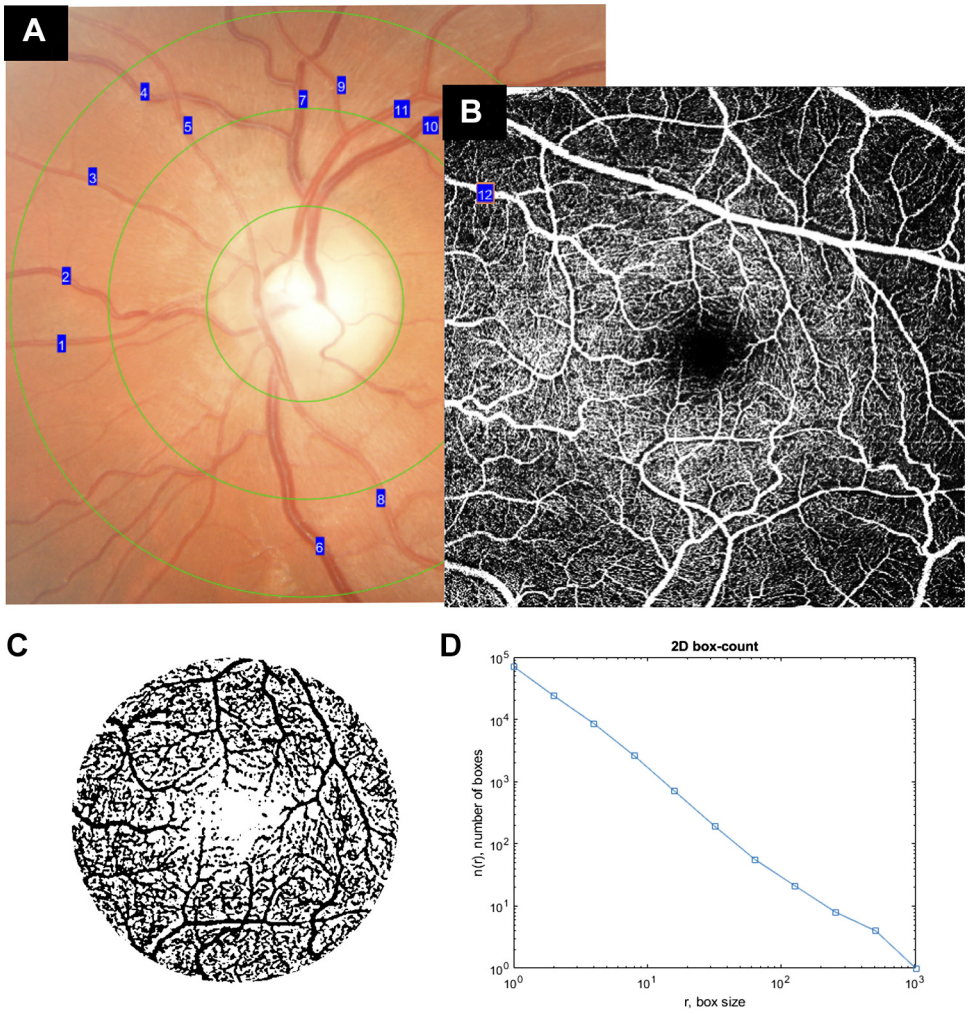

Fig. 1. *A*: cropped 45° fundus image centered at the optic disk. According to the Knudtson-Parr-Hubbard algorithm, the 6 largest arteries and 6 largest veins within the region of interest are marked with blue labels. *B*: overlayed 20° optical coherence tomography angiography (OCTA) image of the superficial vascular plexus of the same eye centered at the macula. *C*: OCTA image from *B* binarized within a 3-mm-diameter circle centered at the macula. Flowing blood vessels, recognized as thresholded pixels, appear in black. *D*: number of superpixels needed to cover the flowing blood vessels plotted against the size of the superpixels in a log-log graph. Fractal ("boxcounting") dimension is equal to the slope of the trend line.

$$\begin{cases} \beta_a = 7.4\left(\frac{\overline{r_{a_0}}}{r_{a_0}}\right)^{\alpha} \\ \beta_v = 7.4\left(\frac{\overline{r_{v_0}}}{r_{v_0}}\right)^{\alpha} \end{cases} \quad (3)$$

Fractal dimension. Fractal dimension (D) is a measure of microvascular complexity. Subjects underwent spectral domain OCT and OCTA imaging (SPECTRALIS Flex Module, Heidelberg Engineering, Inc., Heidelberg, Germany). We calculated D from 20° OCTA images centered at the macula (Fig. 1*B*), by means of customized image processing software. Details and repeatability of this method have been described elsewhere (98). In short, we extracted the vasculature corresponding to the superficial vascular plexus (SVP) from a 3-mm-diameter circle centered at the fovea (Fig. 1*C*), by means of a local Otsu binarization algorithm. Subsequently, we defined D as the Minkowski-Bouligand (boxcounting) dimension:

$$D = \lim_{\varepsilon \to 0} \frac{\log[N(\varepsilon)]}{\log\left(\frac{1}{\varepsilon}\right)} \quad (4)$$

where N and ε describe the number and size of the superpixels needed to cover the vascular area, respectively.

In practice, D can be approximated by the slope of the corresponding log-log plot (Fig. 1*D*).

For the secondary aim of the study, peripapillary retinal nerve fiber layer (pRNFL) thickness and ganglion cell complex (GCC) volume (full 6 × 6 mm ETDRS grid) were also recorded from regular ONH and macular OCT scans.

Blood viscosity (μ). In the retinal microcirculation (where for the Womersley number $Wo < 0.05$ holds, hence viscous forces are much more important than inertial forces), viscosity follows the Fåhræus-Lindqvist effect (30). This effect concerns a decrease in viscosity with a decrease in vessel diameter. Haynes proposed the following formula to account for decreasing radii:

$$\mu(r) = \mu_\infty \frac{r^2}{(r+\delta)^2} \quad (5)$$

where $\mu(r)$ is the viscosity in a branch with radius r, μ_∞ is the asymptotic viscosity in large vessels, and δ is a red-cell-size order of magnitude constant (48).

Kamiya and Takahashi used the data of Fåhræus and Lindqvist to calculate $\delta = 4.29$ μm. μ_∞ can be estimated by the formula of Chien et al.:

$$\mu_\infty = 0.0016209 e^{2.0795\frac{\mathrm{Hct}(\%)}{100}} \mathrm{Pa \cdot s} \quad (6)$$

where Hct is the hematocrit expressed as a percentage (20, 63).

An in vitro study suggested that a multiplication by a factor of 1.08 in *Eq. 6* should be used when calculating venous viscosity, due to differences in shear rates compared with arterioles of the same radius (91). In this study, we did not obtain blood samples; instead, we used

the average Hct values reported in the Gubbio Population Study, stratified for age, gender, and BP status (treated vs. untreated AHT) (21).

Capillary parameters. For the three capillary parameters (r_c, l_c, μ_c), we used the values of Takahashi et al. (128). The radius r_c and length l_c of the capillaries are assumed constant ($r_c = 2.5$ μm, $l_c = 500$ μm); that is, they do not autoregulate or undergo significant structural remodeling. An inverse Fåhræus-Lindqvist effect with an increase in viscosity is expected in branches with a diameter of less than 6 μm, since they are smaller than the diameter of a single red blood cell (117). We assume $\mu_c = 0.0046$ Pa·s.

Ocular perfusion pressure. Ocular perfusion pressure (OPP) is the difference between the pressures in the arterial P_a and venous P_v ends. Mean P_a is usually approximated by 2/3 MAP, where MAP is the mean arterial pressure, calculated as MAP = 1/3 SBP + 2/3 DBP, where SBP and DBP are the systolic and diastolic BP, respectively (78). In this study, we use Takahashi's slightly different definition for mean P_a, being 7/10 MAP − 19.5 mmHg, because it results in a more accurate representation of the pressure in the CRA (3, 128). P_v is taken as equal to the intraocular pressure (IOP). Therefore:

$$\overline{\mathrm{OPP}} = \overline{P_a} - P_v = \left(\frac{7}{10}\mathrm{MAP} - 19.5\right) - \mathrm{IOPmmHg}. \tag{7}$$

The BP was measured twice, in sitting position, immediately before the LSFG imaging, with an automated monitor (BM 85, Beurer medical, Beurer GmbH, Ulm, Germany). IOP was measured with a rebound tonometer (Icare TA01i, Icare Finland Oy, Vantaa, Finland), after the subject had placed his or her chin on the chinrest of the LSFG apparatus.

Model Building

We adopt the dichotomous symmetrical branching structure proposed by Takahashi et al. (128). In our model, the CRA and CRV are the stem generation of the arteriolar and venular generations of radius r_{a_0} and r_{v_0}, respectively. In addition, each generation of radius r_i is a compartment of 2^i parallel, congruent resistors with total resistance R_{a_i} (arterioles), R_{v_j} (venules), or R_c (capillaries) as shown in Fig. 2. In agreement with Takahashi et al., 15 generations (including the stem) of arterioles and 15 generations of venules were needed for the radii to drop to capillary level; in addition, the terminal arteriole is assumed to give rise to 4 capillaries, which then reunite into 1 terminal venule (128). This parallel structure allows R_{a_i}, R_{v_j}, and R_c to be calculated similarly to electrical circuits. We can now compute the first outcome variable, RVR, by summing in series all the arteriolar, venular, and capillary resistive generations. This calculation is provided in APPENDIX A.

We can simultaneously express resistance with Ohm's law, analogously to an electrical circuit:

$$\mathrm{RVR} = \frac{\overline{\mathrm{OPP}}}{\overline{\mathrm{RBF}}} \tag{8}$$

where RBF is the mean retinal blood flow.

From this equation, the second outcome variable, RBF, can be directly calculated.

All image processing and calculations were performed in MATLAB R2018a (The MathWorks, Natick, MA). Scripts are freely available and will be personalized for each OCT device upon request to the corresponding author.

LSFG Imaging

We performed LSFG imaging (RetFlow, Nidek Co., Ltd., Gamagori, Aichi, Japan) in the standard orthogonal (22° by 11°) area centered at the ONH (Fig. 3*A*). Measurements were performed in a dark room, following a break of ~15 min, to stabilize systemic and ocular blood flow variables. As already mentioned, no topical mydriasis was applied. We obtained one reliable scan from each patient; upon detection of blinking or motion artifacts, the scan was repeated. An elliptic region of interest (ROI) was manually set to coincide with the ONH borders, and the area within the ROI corresponding to large vessels was automatically identified by the apparatus based on histogram thresholding. The device acquires 30 frames per second over a 4-s measurement period, and for each pixel, the average MBR of all frames over one heartbeat is calculated. The 10 following waveform metrics were extracted within the ROI: mean velocity in large vessels (MV), flow acceleration index (FAI), skew, fluctuation, heart rate (HR), resistivity index (RI), blowout time, acceleration time index, rising rate, and falling rate. The derivation protocol and the interpretation of these metrics have been described elsewhere (82, 87). In brief, they quantify mean BF velocity (in relative units) and additional characteristics obtained from waveform analysis, which depend on pulsatile BF and vessel caliber.

The separate arterial and venous velocity components can be estimated from the in vivo measurements, by making use of the LSFG velocity information, as well as the cross section of the vessels:

$$\overline{\mathrm{RBF}_{iv}} = \pi\overline{u_{a_0}} r_{a_0}^2 = \pi\overline{u_{v_0}} r_{v_0}^2 \tag{9}$$

where iv is short for in vivo; $\overline{u_{a_0}}$, $\overline{u_{v_0}}$ are the mean velocities in the CRA and CRV, respectively; and r_{a_0}, r_{v_0} have been previously defined, from which it follows that:

$$\frac{\overline{u_{a_0}}}{\overline{u_{v_0}}} = \frac{r_{v_0}^2}{r_{a_0}^2}. \tag{10}$$

Importantly, LSFG was used as an independent experimental validation of the theoretical predictions. As such, it is not part of the theoretical model itself.

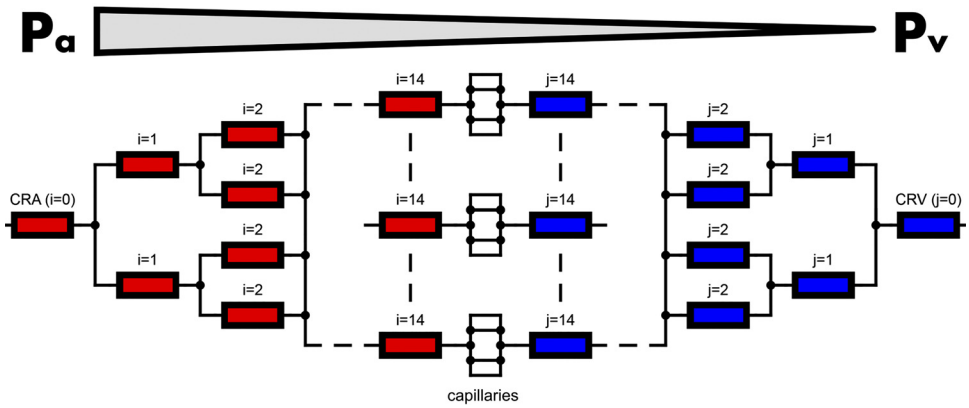

Fig. 2. Geometry of the retinal microcirculatory network, as proposed by Takahashi et al. (128). Dichotomous, symmetric branching is assumed throughout. Central retinal artery (CRA) and central retinal vein (CRV) are set as generation 0 vessels ($i = 0$, $j = 0$). Generation 14 corresponds to the terminal arterioles/venules, each 1 being connected with 4 true capillaries. Flow is driven by the difference between pressures at the arteriolar (P_a) and venular level (P_v).

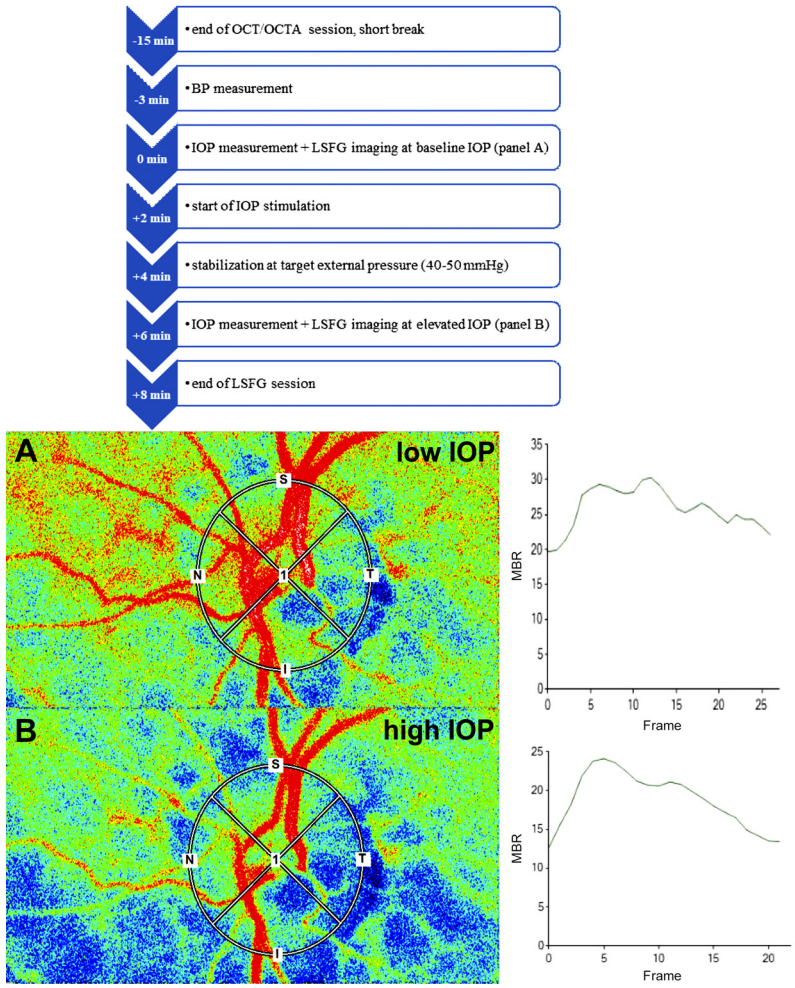

Fig. 3. Laser speckle flowgraphy (LSFG) snapshots of the same eye as in Fig. 1, centered at the optic disk. Graphs on the right display the mean blur rate (MBR) during 1 heartbeat, averaged from all pixels within the region of interest. Pixels with higher MBR are colored in red and correspond to higher blood velocity. Pixels with lower MBR are colored in blue. *A*: LSFG snapshot obtained at baseline venous pressure (P_v), with intraocular pressure (IOP) at 11 mmHg. *B*: LSFG snapshot of the same eye obtained at high P_v, after controlled increase of IOP to 21 mmHg. OCTA, optical coherence tomography angiography; BP, blood pressure.

IOP Stimulation

We used a subset of the study population ($n = 12$, of which 5 subjects had AHT and 1 had both glaucoma and AHT) to repeat the LSFG measurements following IOP increase by means of IOP_{stim} (IMEDOS Systems GmbH, Jena, Germany). Defined external pressure (40–50 mmHg) was applied directly to the sclera at the lateral canthus proximity, while the subjects still had their chin placed on the LSFG apparatus and were gazing forward; IOP was measured again with rebound tonometry. LSFG imaging was repeated with the same laser intensity and at the same location, as registered by the device itself (Fig. 3*B*), within 2 min of established IOP elevation (which itself was reached within 2 min after the onset of stimulation). The metrics described in *LSFG Imaging* were extracted for comparison.

Data Analysis-Statistics

Correlation of model predictions with in vivo blood flow metrics. Multivariable linear regression was performed to examine the relationship between each theoretical model output (either RVR or RBF; dependent variable) and the 10 LSFG waveform metrics (before IOP stimulation; independent variables). By contrast to RBF, where OPP is already incorporated in the theoretical calculation (*Eq. 8*), the regression model for RVR additionally contained MAP and IOP as independent variables. Initially, two saturated models (1 for RVR and 1 for RBF) were built, and subsequently, backward elimination was implemented in each model. Specifically, the least significant variable was removed, and the models with and without this variable were compared using the Akaike Information Criterion (AIC). If the model without the concerning variable had a lower AIC, the same process was repeated for the next least significant variable. The procedure was terminated when the minimal AIC was reached (reduced model). For both reduced models, the coefficient of determination (R^2), regression coefficients, and *P* values were reported.

We also rebuilt the theoretical model replacing the formula by Haynes et al. (see METHODS, *Model Variables and Parameters*, *Blood viscosity* (μ), and *Capillary parameters*) with two alternative viscosity calculations proposed by Pries et al. (Supplemental Material S1: see https://doi.org/10.6084/m9.figshare.12674033.v1) (107, 108, 115). The in vivo viscosity calculation accounts for the presence of the endothelial glycocalyx, while the in vitro viscosity calculation does not (115). We subsequently performed the same fitting analysis, to assess robustness against assumptions related to viscosity.

Contribution of the various factors to the theoretical model. Subsequently, a sensitivity analysis was performed for the model variables contributing to the theoretical model, in two different ways. First, to assess how strongly each contributing variable (vessel radius, viscosity, etc.) affects the outcome values, two new linear models (1 for RVR and 1 for RBF) were built, now using the model input variables as predictors. We directly looked at the magnitude and statistical significance of the standardized regression coefficients in the saturated models to assess the importance of each predictor. Since the more linear the relationships the more accurate results this method yields, we first transformed the independent variables by using *Eqs. A6* and *8* (for example, if variable x contributes as x^{-1} to RVR, it is entered as x^{-1} in the regression analysis) (113). For the second sensitivity analysis, to assess how important (or redundant) each variable is to the model fit, we

recalculated the theoretical predictions with consecutive, independent imputations of the input variables to constant values, one at a time. The constant values assigned were either average values coming from our study sample or theoretical expectations. The new RVR and RBF were fitted again over the LSFG metrics, and the resulting R^2 was successively compared with the ones corresponding to the original models.

Autoregulation. Our in vivo investigation of the RBF model was based on a regression analysis of RBF versus the LSFG variables. In this analysis, OPP, which is part of RBF (*Eqs. A6* and *8*), was based on an assumed contribution of MAP (a factor of 0.70) and on IOP (*Eq. 7*). A presumably more accurate estimate of MAP contribution can be obtained from the investigation of the RVR model, which was based on a regression analysis of RVR versus the LSFG variables, MAP, and IOP. The resulting regression coefficient of MAP was used to optimize the perfusion pressure calculation. Specifically, according to *Eqs. 7* and *8*, a 1-mmHg increase in MAP, holding RBF constant at its central value of x μl·min^{-1} (assuming perfect AR), should produce a $0.7x^{-1}$ mmHg· min·μl^{-1} increase in RVR. If now the RVR regression model predicts a y mmHg·min·μl^{-1} increase in RVR per mmHg increase in MAP (with y the regression coefficient of MAP), this would correspond to a MAP factor of xy in the OPP calculation (instead of 0.70 as used in *Eq. 7* or 0.67 as in the classical OPP definition). The resulting optimized OPP was called retinal perfusion pressure (RPP). The constant (−19.5 mmHg in *Eq. 7*) was subsequently updated to ensure that RPP = OPP (as in the OPP definition implemented in our study), so that the magnitude of RPP still accurately reflects the magnitude of the pressure in the CRA. To verify optimality, we refitted the RBF values (now calculated from RVR and RPP rather than from RVR and OPP) over the LSFG metrics and compared the resulting R^2 with the original.

We then used RPP and our subjects' (excluding glaucoma subjects) vessel characteristics to theoretically calculate the AR limits. For each subject, the lowest and highest AR limits (LARL and HARL) were calculated. This was done for normotensive ($LARL_N$/$HARL_N$) and hypertensive ($LARL_H$/$HARL_H$) subjects separately. Starting with a subject's own RBF calculated from his or her own r_{a_0} and RPP, $LARL_N$ ($HARL_N$) was defined as the RPP needed to keep RBF constant at simultaneously maximal (minimal) r_{a_0} and minimal (maximal) β_a, as observed in the normotensive sample, ceteris paribus. Similarly, we defined $LARL_H$ ($HARL_H$) for the hypertensive subjects. More details on this calculation can be found in Supplemental Material S2A (see https://doi.org/10.6084/m9.figshare.12738590.v1). Glaucoma subjects were excluded from this analysis because, in these subjects, perfect AR is less safe as an assumption (12, 114).

We also examined the ability for AR on the basis of the LSFG in vivo measurements prior and during stimulation. First, Wilcoxon signed-rank tests with the Bonferroni correction were used for individual comparisons of all relevant LSFG metrics (i.e., metrics that stayed in at least one of the reduced RVR or RBF models), before and during IOP elevation. Next, we studied the effect of IOP elevation on RVR and RBF. In the absence of vessel diameter measurements during IOP elevation, RVR_{stim} was approximated using the reduced RVR model (see METHODS, *Data Analysis-Statistics*, *Correlation of model predictions with in vivo blood flow metrics*). RBF_{stim} was then calculated from *Eq. 8*. First, we used Wilcoxon signed-rank tests to compare RVR_{stim} with baseline RVR and RBF_{stim} with baseline RBF. Ideally, that is, within AR limits, RVR would change in response to stimulation, yielding an unchanged RBF. However, if the IOP elevation will bring a subject below LARL, RVR will change less than expected and RBF will show some decrease. To further explore this, we defined AR reserve (AR_{res}) to this stimulation (maximal percentage of RPP change that can be induced by the stimulation), being:

$$AR_{res} = \frac{RPP - LARL}{RPP} 100\% \quad (11a)$$

for those subjects where the stimulation went below LARL. For those who stayed within the autoregulation range, the relevant change in RPP (AR_{change}) is given by:

$$AR_{change} = \frac{RPP - RPP_{stim}}{RPP} 100\%. \quad (11b)$$

We used Spearman's rank correlation coefficient (ρ) to examine to what extent the percentage change in RVR is influenced by the AR reserve/change of each subject (again, excluding glaucoma subjects) during this stimulation. Ideally, percent change in RVR plotted against percentage AR reserve/change should yield datapoints scattering around the minus identity line.

Similarly, we defined the AR deviation (AR_{dev}) to this stimulation (percentage of "below LARL" change induced by the stimulation), according to the following equation:

$$AR_{dev} = \frac{LARL - RPP_{stim}}{LARL} \%. \quad (11c)$$

For those subjects where the stimulation went below LARL, AR deviation will be positive, whereas it will be zero or negative in those where the IOP stimulation respects LARL. The same correlation analysis as in the previous paragraph was performed, this time for percent change in RBF versus AR deviation.

Blood flow and retinal layer thicknesses. Lastly, as a secondary analysis, we examined the relationship of RBF with the thickness of the pRNFL and the volume of the GCC of the same eyes by means of age-adjusted linear regression models. For comparison, the regression model with the original RBF calculation as predictor and the regression model with the optimized (RPP-based) RBF calculation as predictor are both reported.

Normally distributed variables are described by mean (SD), while skewed variables are described by median (interquartile range [IQR]). All analyses were performed in R (version 3.4.2; R Foundation for Statistical Computing, Vienna, Austria). $P \leq 0.05$ was considered statistically significant. For nested models, AIC-based inclusion in the model implies $P < 0.16$ (52).

RESULTS

General Characteristics

Table 1 summarizes the characteristics of the population on which the model predictions were tested in vivo.

Relationship with In Vivo Data

Table 2 displays the reduced multivariable models showing the relationship of the theoretical predictions with the in vivo LSFG measurements. LSFG metrics are obtained by operations in MBR relative units (see METHODS, *LSFG Imaging*). Holding other variables constant, a one MBR-unit decrease in MV results in an increase of 0.015 mmHg·min·μl^{-1} in RVR. In the same model, an increase in FAI and MAP and a decrease in *skew* and fluctuation result in an increase in resistance. Interestingly, IOP is not present in the reduced RVR model. Similarly, holding other variables constant, a one MBR-unit increase in MV results in an increase of 0.7 μl·min^{-1} in RBF. In the same model, a decrease in FAI and HR and an increase in skew result in an increase in BF.

According to the R^2, 77% and 56% of the variation in the theoretical values for RVR and RBF, respectively, could be explained solely by the LSFG waveform metrics. Supplemental Table S1 (Supplemental Material S1: see https://doi.org/10.6084/m9.figshare.12674033.v1) is similar to Table 2, after implementation of alternative viscosity calculations (see METHODS, *Data Analysis/Statistics*, *Correlation of model predictions with in vivo blood flow metrics*). Similar proportion of variation for RVR and RBF could be explained by LSFG metrics; RVR and RBF values

Table 1. *Characteristics of the population used for in vivo investigation*

General characteristics	
Age, yr [median (IQR)]	54 (47 to 56)
Sex, %Female	69.4
BMI, kg·m^{-2} [mean (SD)]	27.5 (5.6)
AHT	
Prevalence, %	41.7
Use of antihypertensive medication, %	73.3
Glaucoma	
Prevalence, %	13.9
Use of antiglaucoma medication, %	100.0
Visual field MD, dB [median (IQR)]	−4.4 (−8.8 to −1.6)
pRNFL, μm [median (IQR)]	103 (92 to 109)
GCC, mm^3 [mean (SD)]	2.79 (0.29)
Theoretical model input variables	
CRAE, μm [mean (SD)]	167 (20)
CRVE, μm [mean (SD)]	239 (21)
β_a [median (IQR)]	7.81 (7.18 to 8.48)
β_v [mean (SD)]	7.77 (0.75)
D [median (IQR)]	1.596 (1.572 to 1.605)
μ_∞ Arterial, Pa s [median (IQR)]	0.0038 (0.0037 to 0.0042)
μ_∞ Venous, Pa s [median (IQR)]	0.0041 (0.0040 to 0.0045)
SBP, mmHg [mean (SD)]	134 (21)
DBP, mmHg [mean (SD)]	83 (12)
IOP, mmHg [mean (SD)]	16.3 (3.8)
Theoretical model outcome variables	
RVR, mmHg·min·μl^{-1} [median (IQR)]	0.71 (0.65 to 0.91)
RBF, μl·min^{-1} [mean (SD)]	45 (12)

Values are as indicated; n = 36. BMI, body mass index; AHT, arterial hypertension; pRNFL, peripapillary retinal nerve fiber layer; GCC, ganglion cell complex; MD, mean deviation; IQR, interquartile range; CRAE, central retinal artery equivalent; CRVE, central retinal vein equivalent; β_a, arteriolar branch length coefficient; β_v, venular branch length coefficient; D, fractal dimension; μ_∞, viscosity in large vessels; SBP, systolic blood pressure; DBP, diastolic blood pressure; IOP, intraocular pressure; RVR, retinal vascular resistance; RBF, retinal blood flow.

remained at the same order of magnitude (Table 1), as did the beta values (Table 2); all beta values kept the same sign.

Figure 4 shows the corresponding scatterplots (rotated residual plots) for RVR (Fig. 4*A*) and RBF (Fig. 4*B*). Visual inspection suggests that subjects with AHT tend to cluster toward higher RVRs than subjects without AHT, as expected; this was confirmed as significant in a Mann-Whitney U test (P = 0.005). RBF was similar for both groups (P = 0.11); that said, when MAP is high, RBF tends to be overestimated by the theoretical model, since most hypertensives (11 of 15) are found below the diagonal line. Indeed, a Wilcoxon signed ranks test revealed that, in hypertensives, the regression-predicted value was on average 5.8 μl·min^{-1} lower than the theoretical model output (P = 0.039).

Sensitivity Analysis

The results of the regression-based sensitivity analysis are given in Table 3. The CRA radius is the most important variable in the RVR calculation (b_{stand} = 0.79, $P = 2.0{\cdot}10^{-29}$), while MAP is the most important variable in the RBF calculation (b_{stand} = 1.06, $P = 8.6{\cdot}10^{-13}$). The magnitude of RBF is not really affected by venular diameter and fractal dimension. For both sensitivity models, we merged each vessel caliber predictor with the corresponding branch length coefficient into one single predictor (e.g., $\beta_a r_a^{-4}$) and additionally, we did not differentiate viscosity in arteries and veins, to avoid collinearity issues (see *Eqs. 3* and *6*).

Table 3 demonstrates the extent to which imputations affect the model fit. The new RVR and RBF models that demonstrated the smallest fit were the ones with all fundus variables imputed with −22% and −24% of variance explained, respectively, compared with baseline. Imputation of solely the branch length coefficient resulted in a small increase in the RVR fit (+3%) but a more substantial drop in the RBF fit (−10%). The variable whose imputation induced the smallest change from baseline was fractal dimension (−2% and −3% for RVR and RBF, respectively).

Figure 5 displays the tornado plots corresponding to the RVR and RBF models. RVR and RBF are displayed as a function of the full dynamic range (minimum to maximum, as observed in our study sample) of each individual component. As shown in the RBF plot, the MAPs of our sample would be able to produce a wide RBF dynamic range (25.0 μl·min^{-1} to 80.1 μl·min^{-1} around the central value of 47.5 μl·min^{-1}), ceteris paribus. For visualization purposes, variables in the figure are permitted to vary independently; however, as expected, the arterial diameter is, in fact, dependent on MAP (Pearson's r = −0.46, P = 0.004); together with the collinear arterial branch length coefficient, they have an important, compensatory effect on RBF values (see METHODS, *Data Analysis*/*Statistics*, *Autoregulation*).

Retinal Perfusion Pressure

Since OPP is only an approximation of the pressure difference between the arterial and venous components of the retinal circulation, we additionally looked for the RPP that optimizes the RBF model fit. This is given by the following formula:

$$\overline{\mathrm{RPP}} = \left(\frac{39}{100}\mathrm{MAP} + 10.1\right) - \mathrm{IOPmmHg}. \qquad (12)$$

With this calculation, the new (optimal) R^2 for RBF was 65% (to be compared with the previous 56%). Interestingly, 65% is

Table 2. *Reduced multivariable fitting models for RVR and RBF with LSFG metrics*

	RVR, mmHg·min·μl^{-1}			RBF, μl·min^{-1}		
	β	P value	R^2 (P)	β	P value	R^2 (P)
			0.77 ($6.9{\cdot}10^{-9}$)			0.56 ($3.1{\cdot}10^{-5}$)
MV	−0.015	$1.0{\cdot}10^{-6}$		0.7	$2.1{\cdot}10^{-4}$	
FAI	0.116	$2.2{\cdot}10^{-5}$		−6.5	$2.0{\cdot}10^{-4}$	
Skew	−0.039	$1.0{\cdot}10^{-5}$		2.5	$2.1{\cdot}10^{-5}$	
Fluctuation	−0.026	0.045			NA	
HR		NA		−0.3	0.026	
MAP	0.009	$2.0{\cdot}10^{-6}$			NA	

LSFG, laser speckle flowgraphy; MV, mean velocity in large vessels; FAI, flow acceleration index; MAP, mean arterial pressure; HR, heart rate; NA, not applicable; RBF, retinal blood flow; RVR, retinal vascular resistance.

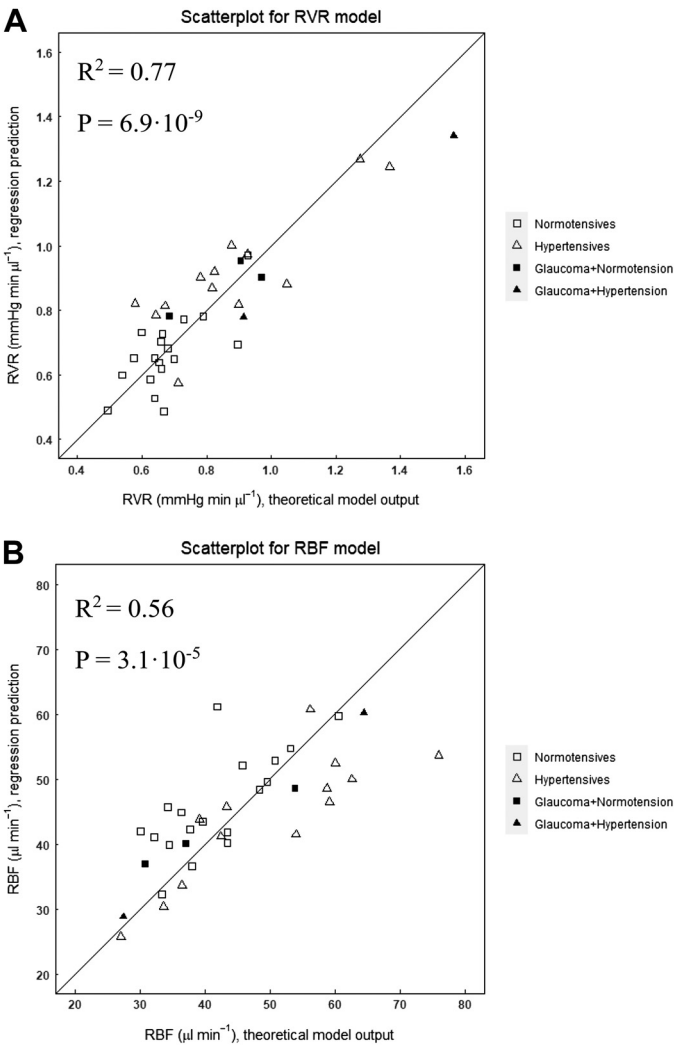

Fig. 4. Scatterplots (n = 36) for multivariable regression models fitting laser speckle flowgraphy metrics to the theoretical output: retinal vascular resistance (*A*; RVR) and retinal blood flow (*B*; RBF). Regression-predicted values (equivalently: theoretical model values minus corresponding residuals) are plotted against the theoretical model values. Diagonal line represents perfect fit (no residuals).

actually the global maximum R^2, given a MAP factor of 0.39, and is achieved at a range of MAP constants containing the predicted +10.1 (+7.7 to +11.1). Lastly, with this RPP calculation, there was no longer an overestimation of the theoretically predicted RBF in hypertensive patients, as seen above (see RESULTS, *Relationship with In Vivo Data*; Wilcoxon signed rank test, P = 0.55).

Autoregulation and IOP Stimulation

Figure 6 displays the theoretically predicted AR plateaus (i.e., the RPP span between LARL and HARL) for each individual nonglaucomatous subject (n = 31), as well as the full AR curves for the average cases with (red) and without (blue) AHT, in healthy eyes. All subjects are autoregulating; hence, as shown in the graph, their baseline status can be found inside their individual plateau. Beyond the AR limits, RBF is proportional to RPP. $LARL_N$ for the average case was estimated from Fig. 6 at 25 mmHg (SD: 4 mmHg). This, according to *Eq. 12*, corresponds to a MAP of 77 mmHg (i.e., a BP reading of 105/65 mmHg) at mean IOP (15 mmHg in the non-AHT group) or to an IOP of 20 mmHg at mean MAP (89 mmHg). In fact, a BP 1 SD below average together with an IOP 1 SD above average brings a subject already at or below $LARL_N$. $LARL_H$ for the average case was estimated at 27 mmHg (SD: 6 mmHg). Similarly, this corresponds to a MAP of 88 mmHg (i.e., a BP reading of 115/75 mmHg) at mean IOP (17 mmHg in the AHT group) or to an IOP of 26 mmHg at mean MAP (111 mmHg). $HARL_N$ and $HARL_H$ were estimated as 39 mmHg (SD: 7 mmHg) and 54 mmHg (SD: 13 mmHg), respectively. This rightward shift of the AR limits in AHT was only significant for HARL according to the Mann Whitney U test (LARL: P = 0.12; HARL: P = 0.001).

After stimulation, IOP increased (hence RPP decreased, assuming MAP remained relatively unchanged) in all 12 subjects by a median of 9 mmHg (IQR: 4.5 to 14.8 mmHg; P = 0.002). Among relevant LSFG metrics (i.e., metrics included in Table 2), MV decreased (P = 0.002), whereas skew and fluctuation increased (P = 0.006 and P = 0.002, respectively). These differences were significant even at the Bonferroni-adjusted threshold of P = 0.01. It is important to mention here that, in univariable analysis at baseline (n = 36), skew was the one parameter most strongly associated with arterial diameter at an interindividual level, and this was in a positive direction (Pearson's $r = 0.59$, $P = 1.6 \cdot 10^{-4}$); age did not play a role in this association, as shown in the bivariable model (P = 0.63). FAI and HR did not change (P = 0.26 and P = 0.45, respectively) after IOP stimulation. Figure 7 depicts changes in skew, MV, and IOP before and after IOP stimulation in individual subjects. Regarding the effect of stimulation on RVR, RVR_{stim} was not significantly different compared with baseline, regardless of whether baseline RVR was calculated from the theoretical variables (P = 0.94) or the regression coefficients in Table 2 (P = 0.75). However, within overall nonsignificance, RVR percent change was more negative with larger AR reserve/change ($\rho = -0.66$, P = 0.026). On the other hand, RBF_{stim} was lower by a median of 17.9 $\mu l \cdot min^{-1}$ compared with baseline (P = 0.019). In addition, RBF percentage change was more negative with larger AR deviation ($\rho = -0.91$, $P = 1.1 \cdot 10^{-4}$). These observations have been visualized in Supplemental Fig. S2*B* (see https://doi.org/10.6084/m9.figshare.12738590.v1).

Resistivity Index

As a secondary observation, RI (which did not appear in the reduced final models) also showed an increase after IOP elevation (P = 0.002). In addition, its baseline value exhibited a correlation with the pulse pressure index (n = 36, Spearman's $\rho = 0.49$, P = 0.002), which is defined according to the following equation:

$$PPI = \frac{SBP - DBP}{SBP} = 1 - \frac{DBP}{SBP}. \quad (13)$$

Blowout score is an additional metric offered by the LSFG but was not considered at all in this study, since it can be directly calculated from the RI. Indeed, our in vivo data also confirmed that the two metrics are collinear (n = 36, Spearman's $\rho = 0.90$, $P = 1.8 \cdot 10^{-13}$). Notably, RI and fluctuation were also highly correlated (n = 36, Spearman's $\rho = 0.87$, $P = 3.8 \cdot 10^{-12}$).

Table 3. *Sensitivity analysis for the theoretical model predictions*

	RVR			RBF			Imputed variable(s)	
	Stand. β	*P* value	R^2	Stand. β	*P* value	R^2	R^2 (RVR)	R^2 (RBF)
Regression-based sensitivity analysis			0.99 $P = 7.1\cdot10^{-33}$			0.88 $P = 6.8\cdot10^{-12}$		
$\beta_a r_a^{-4}$	0.79	$2.0\cdot10^{-29}$						
$\beta_v r_v^{-4}$	0.26	$2.1\cdot10^{-15}$						
$r_a^4 \beta_a^{-1}$				0.76	$2.8\cdot10^{-8}$			
$r_v^4 \beta_v^{-1}$				0.00	0.97			
e^{-D}	0.07	$2.9\cdot10^{-4}$						
e^{D}				0.03	0.70			
μ_∞	0.11	$5.7\cdot10^{-7}$						
μ_∞^{-1}				0.17	0.037			
MAP				1.06	$8.6\cdot10^{-13}$			
IOP				−0.42	$1.6\cdot10^{-5}$			
Imputation-based sensitivity analysis								
Baseline (from Table 2)							0.77	0.56
$r_a = 176$ μm, $r_v = 248$ μm, $\beta_a = \beta_v = 7.4$							0.55	0.22
$\beta_a = \beta_v = 7.4$							0.80	0.46
$D = 1.7$							0.75	0.53
μ_∞(art) = 0.0043 Pa s, μ_∞(ven) = 0.0046 Pa s							0.69	0.49
MAP = 95 mmHg							*NA*	0.38
IOP = 15 mmHg							*NA*	0.41

r_a, central retinal artery radius; r_v, central retinal vein radius; β_a, arterial branch length coefficient; β_v, venous branch length coefficient; *D*, fractal dimension; μ_∞, blood viscosity in large vessels; MAP, mean arterial pressure; IOP, intraocular pressure; NA, not applicable.

Model Predictions and Structural Measurements

Table 4 displays the age-adjusted linear regression models for the relationship between blood supply (RBF) and inner retinal structural measures (pRNFL thickness, GCC volume). In the optimized RBF model, 1 μl·min^{-1} increase in RBF is associated with a 0.69-μm increase in pRNFL and a 0.012-mm^3 increase in GCC. Associations remained significant, albeit weaker, after exclusion of the glaucoma subjects.

DISCUSSION

In this study, we proposed and tested a physiological model, coupled with a clinical protocol, that predicts the behavior of retinal vascular networks on an individual level by means of two clinical markers, RVR and RBF. Investigation in human subjects showed that a considerable proportion of the variation in the theoretical predictions could be explained by in vivo BF metrics, as given by LSFG. MV, FAI, and skew were the LSFG

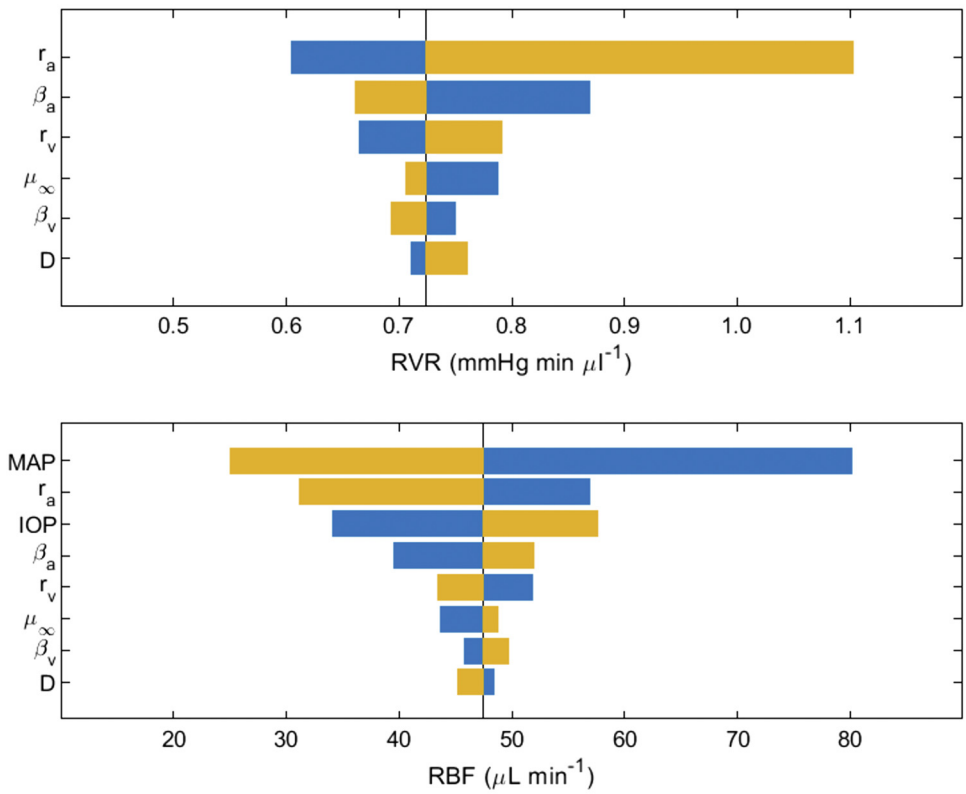

Fig. 5. Tornado plots for the simulated retinal vascular resistance (RVR) and retinal blood flow (RBF) models. Vertical line gives the outcome value at the central value of all predictors. Horizontal bars display the outcome values at the full range of each predictor, all other predictors being at their central value. Blue and orange colors correspond to the high and low values of each predictor, respectively.

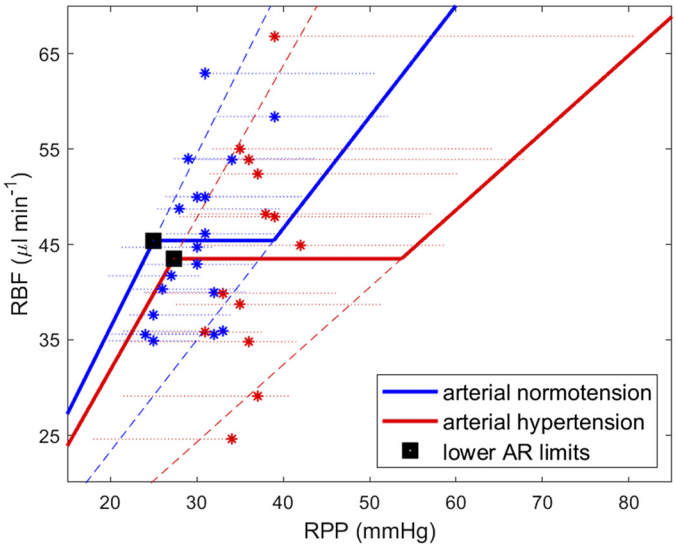

Fig. 6. Predicted autoregulation (AR) curves for arterial normotension (n = 18) and arterial hypertension (n = 13), each centered at mean retinal blood flow (RBF). Dashed lines (extended) meet at the origin. Retinal perfusion pressure (RPP) is calculated according to *Eq. 12*. Star-shape markers denote baseline RBF, as estimated from vascular caliber, viscosity, fractal dimension, and RPP. Dotted lines represent individual AR plateau approximations, extending from the lower to the higher AR limit (LARL, HARL). LARL and HARL for each subject are theoretically predicted, according to a standardized procedure (see METHODS, *Data Analysis-Statistics*, *Autoregulation*). If the subject is close to maximum arteriolar dilation, the baseline marker will be found close to LARL. If the subject is close to maximum arteriolar constriction, the baseline marker will be found close to HARL.

metrics exhibiting the strongest associations with both outcomes. According to the sensitivity analysis, all variables included a priori in the theoretical model were confirmed to range from very important to at least mild determinants of RVR and RBF. Using the model and the in vivo data, we proposed AR curves and predicted LARL for subjects with and without AHT. We then verified that changes in RVR and RBF induced by IOP elevation are, indeed, dependent on the AR reserve/change and AR deviation, respectively. Lastly, we demonstrated that the amount of nerve tissue present in the inner layers of the human retina is strongly correlated with blood supply.

Model Investigation Results: Literature Comparison and Physiological Interpretation

Retinal blood flow and retinal vascular resistance. The proposed model predicted a mean RBF of 45 (12) μl·min^{-1} in our sample (Table 1), which agrees with values reported in the vast majority of studies using Doppler OCT and laser-Doppler velocimetry (24, 37, 41, 76, 119, 139, 141). Older studies using laser Doppler velocimetry reported higher RBF values, possibly because previous hardware versions of this technique overestimated blood velocity (31, 39). Contrary to the previous methods, the LSFG apparatus does not yield an absolute BF estimate; hence, all waveform metrics were a priori given an equal opportunity to be included in the reduced multivariable models (see DISCUSSION, *Laser speckle flowgraphy metrics*).

According to *Eq. 8*, high RVR mathematically implies either high OPP or low RBF. Our results clearly demonstrate this (Table 2), since increased RVR (which reflects narrower arterioles) was associated with an increased MAP, as well as decreased MV, when the other is held constant. To calculate RVR, previous studies relied on first estimating RBF with one of the aforementioned, usually challenging, dynamic techniques and then applying *Eq. 8* (64, 90, 94). In our study, we demonstrated that it is possible to quantify resistance by static imaging and simple clinical examinations, without any information on BF as a prerequisite. After RVR is constructed from its individual components, RBF can be obtained with a simple calculation from *Eq. 8*. In this regard, RI, which is calculated according to the following formula:

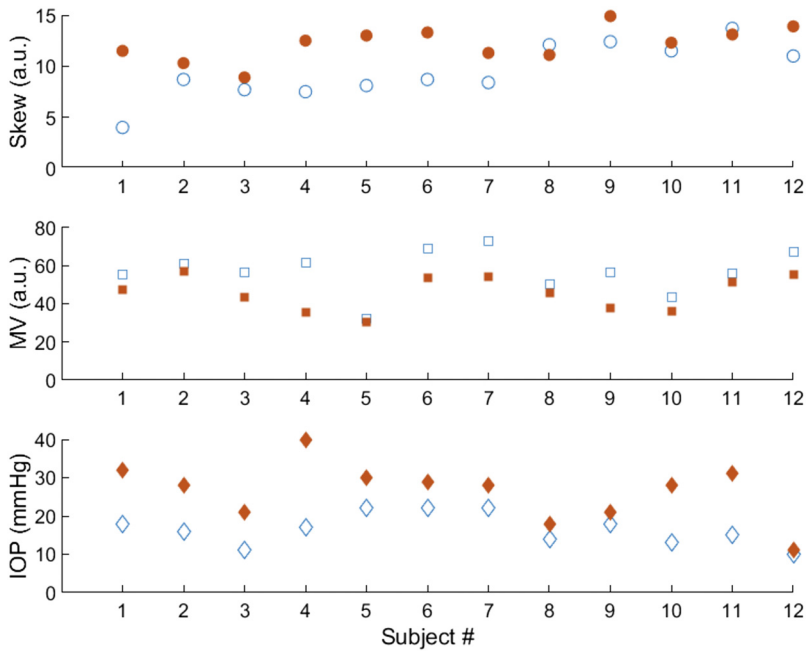

Fig. 7. Skew, mean velocity in large vessels (MV), and intraocular pressure (IOP) values in individual subjects (n = 12) plotted before (empty blue markers) and after (filled red markers) IOP stimulation. Subjects are ranked from highest to lowest autoregulatory (AR) reserve/change (*Eqs. 11a* and *11b*). *Subject 5* is a primary open angle glaucoma subject. Wilcoxon signed-rank tests revealed simultaneous increase in skew and decrease in MV, following IOP elevation, which is an indication of AR capacity with conservation of flow; a.u., arbitrary units.

Table 4. *Age-adjusted linear models for structural SD-OCT metrics as a function of RBF*

	pRNFL, μm			GCC, mm^3		
	β	*P* value	R^2 (*P*)	β	*P* value	R^2 (*P*)
Models with original RBF calculation			0.46 ($3.7{\cdot}10^{-5}$)			0.35 (0.001)
RBF, $\mu l{\cdot}min^{-1}$	0.53	0.002		0.009	0.011	
Age, yr	−0.76	$5.6{\cdot}10^{-5}$		−0.013	0.001	
Models with optimized RBF calculation			0.51 ($7.0{\cdot}10^{-6}$)			0.40 ($4.0{\cdot}10^{-4}$)
RBF, $\mu l{\cdot}min^{-1}$	0.69	$4.0{\cdot}10^{-4}$		0.012	0.003	
Age, yr	−0.65	$1.8{\cdot}10^{-4}$		−0.011	0.003	

pRNFL, peripapillary retinal nerve fiber layer; GCC, ganglion cell complex; RBF, retinal blood flow; SD-OCT, spectral domain optical coherence tomography.

$$\mathrm{RI} = \frac{u_{\max} - u_{\min}}{u_{\max}} = 1 - \frac{u_{\min}}{u_{\max}} \qquad (14)$$

where u_{max} and u_{min} are the peak systolic velocity (PSV) and end diastolic velocity (EDV), respectively, has been previously shown to not be an adequate standalone representation of vascular resistance. Instead, it reflects combined effects of resistance and compliance, a phenomenon that has also been observed in the circulation of other organs (9, 51, 95, 103). Our data second that: first, fluctuation, which is a more detailed computational quasiequivalent highly correlating with RI, possibly masked the effect of RI in the reduced multivariable RVR model and still was only of borderline significance (Table 2). Moreover, the strong correlation between RI and PPI that we replicated suggests that RI also depends on central impulse, in addition to downstream flow characteristics (1).

Laser speckle flowgraphy metrics. Overall, LSFG metrics explained considerable proportion of variance in the RVR and RBF calculations, exhibiting some very strong correlations in multivariable analysis (Table 2). This suggests that the theoretical approximations implemented in this study were able to capture individual variations in blood flow physiology, as measured in vivo. In this subsection, we discuss the physiological meaning of each (significant) LSFG component and its relationship with the theoretical predictions.

MV represents blood velocity in large retinal vessels, which, according to *Eq. 9*, is a primary component of RBF and is segmented separately from the signal of surrounding tissues (16, 50). It also incorporates information from both the arteriolar and venular component; hence, it is informative in conditions where velocity is affected due to changes in vascular caliber (e.g., in glaucoma). For these reasons, it has been used as a surrogate for BF in a number of LSFG studies (60, 61, 81, 87). In particular, Iwase et al. showed that OPP reduction by means of IOP stimulation induced a drop in MV, a finding that was also confirmed in our study. In addition, another study revealed that MV was significantly lower in normal tension glaucoma (NTG), compared with healthy controls (87). These findings suggest that MV is sensitive to both physiological and pathological BF changes. We note here that, in our study, there was no correlation between MV and ONH size (Pearson's $r = -0.08$, $P = 0.62$) and that ONH size did not confound any of the associations uncovered in the reduced multivariable LSFG models. Hence, there was no artifactual component related to the area of measurement in the MV-driven associations.

According to *Eq. 9*, a predictor related to vessel diameter was also reasonably expected to show up in the models, after adjusting for MV (Table 2). Skew was the LSFG metric that best reflected arteriolar caliber, since it was the predictor that was most strongly, positively associated with CRAE in univariable analysis (and also bivariable age-adjusted analysis), as well as negatively with RVR and positively with RBF in the reduced multivariable models. In addition, skew significantly increased after IOP elevation, with a concomitant decrease in MV, most likely indicating AR-driven vasodilation with conservation of flow (Fig. 7). Results from other LSFG studies corroborate this finding. Shiga et al. showed a decrease in skew in NTG, compared with controls, while Gardiner et al. found the same effect when comparing POAG patients to controls, only when the eyes had detectable functional deficit (40, 116). Additionally, Bhatti et al. reported a mild increase in skew 40 min after challenging IOP with the water drinking test in healthy individuals (11). They did not report IOP values before and after the challenge, but this test is expected to increase IOP by 3–4 mmHg (126). However, the opposite effect was observed by Kiyota et al., with skew decreasing after a 20-mmHg controlled IOP elevation, with a procedure similar to ophthalmodynamometry (70). This discrepancy with our data could possibly be explained as follows: first, such a big IOP increase is unlikely to have been confined within the AR limits in most of their subjects (Fig. 6), as such, decreased skew in this case might indicate decreased RBF more than it indicates increased RVR. In addition, the compressive force exerted by high IOP to passively reacting venules and capillaries (and at very high IOP, even arterioles, as was suggested in a recent study) might partly cancel out the AR effect of arterial vasodilation (92, 109). Lastly, Kiyota et al. obtained measurements from the ONH tissue area, not including the large retinal vessels; this area is characterized by more complex vascular supply and, therefore, might exhibit different AR properties (70, 106). Despite the multiple indications present in our data, we believe that additional studies are needed to clarify the relationship between skew and arteriolar caliber.

In addition to MV and skew, increased FAI was found to be an independent predictor of higher RVR and lower RBF (Table 2). There are a number of explanations for this commonly reported phenomenon (22, 112, 125). First, the shear stimulus for flow-mediated dilation (FMD) is known to also depend on flow acceleration, triggering a transient initial burst of nitric oxide (NO) production at the endothelium, before the slower NO release attributed to flow velocity (122, 123). Specifically, increased acceleration is expected to attenuate FMD. Second, flow acceleration in the microcirculation exhibits a more complex behavior than in the macrocirculation. Indeed, in large vessels, where the effects of inertance on flow acceleration dominate the effects of resistance on flow velocity, Newton's second law of motion is generally sufficient for an estimate of

acceleration (115). We illustrate this in APPENDIX B. However, Doppler ultrasound studies in other organs revealed that, downstream in the circulation, increased distal resistance is associated with higher early systolic acceleration, possibly due to interference of reflections with the dampened wave (47, 125). To our knowledge, this is the first study to demonstrate that this phenomenon holds true in the ocular circulation, since FAI was positively associated with RVR in the reduced model (Table 2). Lastly, flow acceleration can introduce an error in velocity measurements, especially in stenotic segments or areas of turbulent flow (73, 97). Hence, adjusting for an acceleration term in the RVR and RBF models is expected to increase precision. This artificial normalization could also be especially beneficial for reducing variability in LSFG measurements, where univariable interindividual comparisons are difficult to interpret, due to the effect of pigmentation (89). Notably, again shown in the APPENDIX B, the presence of FAI in the model also provides an explanation for the in vivo documented differential effect of distal resistance on PSV and EDV values, which sometimes can even lead to diastolic flow reversal (47).

Univariable analysis in the study of Gardiner et al. showed increased FAI in early POAG, compared with controls, but only in eyes with no detectable functional deficit; FAI values dropped back to baseline when functional deficit was present (40). Another study revealed decreased FAI in NTG, compared with controls (87). At first, this seems paradoxical, as it points toward lower RVR and higher RBF, while the opposite is expected (148). However, in our multivariable regression models (Table 2), interpretation of these effects required other LSFG metrics to be held constant. Indeed, using the regression coefficients in Table 2 and the average values for LSFG metrics provided in their study, we reverse-engineered approximations for average RVR and RBF values in their population: 0.77 mmHg·min·μl^{-1} and 50.5 μl·min^{-1} for NTG patients, versus 0.59 mmHg·min·μl^{-1} and 54.3 μl·min^{-1} for controls. These values reflect the physiological expectations and are somewhat comparable to the average values we report, despite the fact that they used a different LSFG apparatus, yielding considerably different MBR values. We invite researchers to use this approach to reanalyze their LSFG data.

A faster HR was also weakly associated with reduced RBF (Table 2). Womersley's model for oscillatory BF predicts that, in large vessels, HR would affect maximal, but not average, BF during the cardiac cycle (144). In the microcirculation, where Womersley number Wo is small and BF tends to approximate steady-state behavior, HR is theoretically not expected to profoundly influence BF. That said, it is apparent from the LSFG waveforms (Fig. 3) that retinal BF still has a transient component. In addition, peripheral resistance has been shown to not be an accurate representation of impedance at nonzero frequencies, because of wave reflections and the fact that viscous drag increases with increasing oscillation frequency (7, 46). These observations could explain our findings.

Quantitative Vascular Analysis: Literature Comparison and Physiological Interpretation

In the sensitivity analysis, the CRAE (r_a) was the most important variable in determining RVR and the second most important (after MAP) in determining RBF (Table 3 and Fig. 5). This is not unexpected, since it is mostly the arterioles that are responsible for short-term (AR) or long-term (structural remodeling) control of circumferential wall stress, in response to acute or chronic changes in perfusion pressure (77, 111). In this study, we estimated vascular caliber from fundus images. Semiautomatic retinal vascular caliber measurements have not been fully standardized and are known to be influenced by the measurement software and the choice of formula (53, 147). We used the most widely accepted Parr-Hubbard formulas, revised by Knudtson et al.; the CRAE and CRVE mean values and ranges observed in our study sample agree with the outcomes of the Beaver Dam Study, when the same formulas are applied (71). They also agree with the values reported by Dorner et al., who used a reverse approach to quantify diameters from flow values (27). We excluded eyes with high refractive error, to keep variability introduced by magnification to a minimum. Upon imputation of central retinal vessel caliber values in the theoretical model, a significant proportion of variance in the in vivo data could no longer be explained (Table 3). This highlights that the use of individualized values is paramount, despite the fact that the indirect caliber estimation of the otherwise inaccessible central retinal vessels could introduce some degree of uncertainty to the model predictions.

It is worth noticing here that the formulas by Knudtson et al. are derived by extracting the branching coefficient B (also known as area expansion ratio) from human retinal vessel bifurcations, a quantity that is calculated as follows:

$$B = \frac{r_S^2 + r_L^2}{r_P^2} \tag{15}$$

where r_S is the small daughter branch, r_L is the large daughter branch, and r_P is the parent trunk. Let us also define an asymmetry index I as:

$$I = \frac{r_S}{r_L}. \tag{16}$$

Using *Eq. A3*, as well as the fact that the number of terminal vessels corresponding to a mother vessel upstream is always equal to the sum of the terminal vessels corresponding to each of the two daughters, Kamiya and Takahashi obtained (63):

$$r_P^{D+\alpha} = r_S^{D+\alpha} + r_L^{D+\alpha}. \tag{17}$$

From *Eqs. 15*, *16*, and *17*, we get (after some algebra):

$$B = \frac{I^2 + 1}{(I^{D+\alpha} + 1)^{\frac{2}{D+\alpha}}}. \tag{18}$$

Pooled data from the studies of Knudtson et al. and Patton et al. suggest that B is ~1.27 [confidence interval (CI): 1.21 to 1.33] for arterioles and 1.15 (CI: 1.10 to 1.21) for venules (71, 100). Moreover, Aschinger et al. provided mean (SD) values for the bifurcation exponent (here $D + \alpha$) using a power fitting approach based on data from Doppler OCT (5). A value of 3.01 (0.22) was proposed for arterioles, while 2.62 (0.26) was proposed for venules. When no differentiation is made between arterial and venous bifurcation exponents, Murray's law predicts a value of 3.00, based on a minimum work principle, while Takahashi et al. suggest an exponent of 2.85 based the theoretical values $D = 1.70$ and $\alpha = 1.15$ (86, 128).

Our study assumes symmetrical dichotomous branching ($I = 1$), as well as equal $D + \alpha$ (median: 2.75) for arterioles and venules (since, at the moment, microvessels are not differentiated by OCTA). For the sake of comparison, we calculated B using these values, yielding 1.21 (exactly halfway between the arteriole and venule values, pooled from the studies of Knudtson et al. and Patton et al.) (71, 100). In addition, Popel showed that, although heterogeneous models are more precise in accounting for flow rate within individual branches of the same tree, a symmetric series-parallel network is not inferior when it comes to mean total flow predictions (104). These observations together suggest that, since in our study the required outcomes were (or were derived from) total blood flow and total resistance, the branching structure implemented can be considered as equivalent to more complex networks. Notably, according to Patton et al., asymmetry index I is roughly 0.76 for arterioles and 0.75 for venules, when calculated from the first few generations (100). This is indeed high, but still indicates at least some degree of asymmetry, when based on upstream vessels. However, in APPENDIX C, in support of the aforementioned, we provide a mathematical argument as to why asymmetry in the upstream branches is not expected to profoundly affect our main end points. In the same argument, we use a simple optimization principle to justify why, as we move toward the terminal vessels, branching is reportedly less asymmetric than upstream (84). In any case, previous research indicates that, at this terminal level, total flow rate has mostly been determined by the upstream arterioles (84).

Autoregulation: Literature Comparison and Physiological Interpretation

Retinal perfusion pressure. After RVR is obtained, RBF calculation significantly relies on an accurate OPP estimate. In the classical OPP definition, Pa $\approx$ 2/3 MAP is assumed (see METHODS, *Model Variables and Parameters*, *Ocular perfusion pressure*), according to ophthalmodynamometric guidelines; Stodtmeister et al. recommend an additional age correction to account for arterial stiffening, thus avoiding OPP underestimation in the elderly (120, 135). However, it is known that the arterial pressure measured by ophthalmodynamometry actually reflects the pressure somewhere upstream, in the much larger ophthalmic artery, rather than in the CRA (140). Werff estimated the pressure in the CRA to be roughly 14–17 mmHg lower, due to the large pressure gradient produced by its small lumen; in this study we initially used the offset suggested by Takahashi (19.5 mmHg) (128). Comparing *Eq. 12* to 2/3 MAP-IOP, our results suggest that this offset is more likely MAP dependent (rather than constant, as assumed in the aforementioned studies), which is also intuitive, since subjects with AHT should exhibit higher pressure drops from the ophthalmic artery to the CRA. The same phenomenon has also been predicted for cerebral vessels of similar diameters (13). Also pointing toward the superiority of the optimized calculation, results in Table 4 suggest that its implementation also improves the accuracy in pRNFL and GCC predictions. At this point, we should highlight that IOP was not a significant predictor in the reduced RVR model (Table 2), suggesting it might not be a satisfactory surrogate for P_v. This is supported by the observation that the RBF model fit (which includes IOP in the calculation) was worse than the RVR model fit, even after optimizing the OPP formula for P_a. Indeed, several studies report discrepancy between IOP and CRV pressure (the latter is always higher) in patients with glaucoma (or other ocular diseases), vascular dysregulation, and metabolic syndrome but also in healthy subjects with no spontaneous venous pulsation, as well as animal models (6, 32, 68, 88, 121).

Estimation of AR limits. When generating AR curves, we distinguished between subjects with and without AHT. Indeed, there is evidence (mostly coming from the cerebral circulation) that structural remodeling due to AHT shifts the curve to the right, because of the higher transmural pressures needed to achieve a given value of circumferential wall stress (10, 49, 102). This shift was observed in our data, albeit only reaching significance for HARL. AR plateaus are assumed flat in our study (Fig. 6); hence, AR limits are strictly defined: they are the marginal pressures slightly below or over which a minute decrease or increase in RBF is expected to take place (or equivalently the pressures corresponding to maximal vasodilation or vasoconstriction). For the sake of comparison, we also calculated $LARL_N$ and $LARL_H$ using the suboptimal, classical OPP definition at 37 mmHg and 43 mmHg, respectively. Most experimental studies in the literature use binned data and define the AR limits to be the pressures below or over which either a statistically significant or predetermined percent change from baseline BF is observed (109, 110, 131, 143). As such, these studies likely result in a looser LARL and HARL estimation; thus comparisons between these numbers and the predictions of this study are to be interpreted with caution. For example, in the Doppler-OCT study by Puchner et al. ($n = 15$), their Fig. 5 indicates that the drop in BF after IOP elevation only becomes statistically significant at OPP $\simeq$23 mmHg, when, at that point, BF has been reduced by almost 40% (109). However, their data show that AR might not be in effect already at OPP $\simeq$38 mmHg (in agreement with our prediction of 37 mmHg), upon appearance of the steep linear slope expected from *Eq. 8* (Fig. 6). Similarly, in the LSFG study of Witkowska et al. [this time regarding HARL in normotensive subjects ($n = 27$)], Fig. 6 suggests that AR starts to fail when OPP $\simeq$60 mmHg [which almost coincides with our $HARL_N$ prediction, calculated according to the classical OPP definition (58 mmHg)], this time reaching significance almost immediately (OPP $\simeq$62 mmHg) (143).

As expected (see RESULTS, *Autoregulation and IOP Stimulation*), percent change in RVR correlated negatively with AR reserve/change (*Eqs. 11a* and *11b*); similarly, percent change in RBF correlated negatively with AR deviation. These observations verify that the retinal vessels are an autoregulating system and also provide evidence in favor of the specific AR limit approximation implemented in this study. Indeed, we showed that the predicted LARL dichotomizes the perfusion pressure range: below LARL, perfusion pressure drives BF; conversely, above LARL (while below HARL), perfusion pressure drives resistance. However, RVR_{stim} was not significantly different from RVR: this could be due to a simultaneous increase in resistance during IOP elevation, due to the compressive effect of IOP in retinal venules taking over (see next paragraph), or it could indicate that, in the majority of subjects, AR_{res} is close to 0 (i.e., the subject is already close to its LARL). From a teleological point of view, this could imply that most eyes are better prepared to counteract rises in RPP (for example related to physical activity, stress, diet, etc.), rather than RPP drops, being closer to LARL than to HARL (Fig. 6). This is also intuitive given the skewed distribution of BP: larger deviations from the mean are to be expected due to increases in BP. The fact that subjects are usually closer to LARL than to

HARL and are better prepared for transient hypertension than hypotension has been observed in the cerebral circulation (4, 15, 23).

Comparison with Previous Physiological Models

For the sake of comparison with other models, we also calculated the average (SD) velocities in the CRA and CRV, according to *Eq. 9*: 3.3 (0.5) cm/s and 1.6 (0.3) cm/s, respectively, in line with values reported in the literature (101). The observation that venous velocity is roughly one half of the arterial velocity is a consequence of *Eq. 10* and was also confirmed by Malek et al. by means of a fundus-based mathematical model (83).

Following IOP elevation, we reported a decrease in MV, mostly due to conservation of flow after AR-induced vasodilation. Guidoboni et al. showed that this decrease can be also partially attributed to the effect of IOP on the retinal venules (especially when it is considerably above the normal range) and much less to the compressive stress due to the lamina cribrosa (43). This implies that triggering OPP by inducing changes in IOP is not equivalent to inducing changes in MAP; therefore, they might result in slightly different AR responses, a hypothesis that has been confirmed in experimental studies (131, 137). In the mathematical model of Guidoboni et al., Table 2 reports total resistance of 0.71 mmHg·min·μl^{-1} from the CRA to the CRV at the control state, which corresponds to a 28.9-mmHg pressure drop, as reported in Table 3 of the same study (44). These values are in excellent agreement with our median RVR theoretical prediction (0.71 [IQR: 0.65 to 0.91] mmHg·min·μl^{-1}) and the mean RPP (33.1 [SD: 5.1] mmHg), respectively. However, their model relies on a given, mean RBF control value (41 $\mu l\ min^{-1}$), whereas we are additionally able to predict this value on an individual basis, accounting for variations in mean perfusion pressure, vessel caliber, hematocrit, and complexity of the microvascular network. The same study predicted LARLs equivalent to RPP = 24 mmHg and RPP = 23 mmHg for normotensives and hypertensives with intact AR, respectively (to be compared with 25 mmHg and 27 mmHg, respectively, in our study). The 4-mmHg discrepancy in $LARL_H$ between their results and ours is somewhat expected, since they used the same baseline CRA radius for the normotensive and the hypertensive condition. This means their approach describes newly established AHT, before structural remodeling, with the curve exhibiting no rightward shift. Interestingly, their model also predicts an increase in RI following IOP elevation, which we were able to replicate in vivo.

Lastly, Ganesan et al. used the formulas by Pries et al. to demonstrate that taking into account downstream changes in viscosity is paramount to calculating precise pressure drops on the intra-individual level (38, 107, 108, 115). Our model was shown to be robust to the choice of formula (Table 2 and Supplemental Material S1: see https://doi.org/10.6084/m9.figshare.12674033.v1), as long as the same formula is used for all subjects. In our study, we implemented the viscosity corrections by Haynes et al., since the model of Takahashi et al. was built and validated around them (see METHODS, *Model Variables and Parameters*, *Blood viscosity*). Absolute RVR and RBF values resulting from this calculation were more in agreement with previous literature (24, 37, 41, 76, 119, 139, 141). Using these values, we subsequently showed that prediction accuracy increases when interindividual asymptotic viscosity μ_∞ is considered (Table 3) (128). This is further supported by a recent study, showing that blood viscosity was the mediator of sex-related differences in LSFG metrics (61).

Physiological Implications and Clinical Relevance

To the best of our knowledge, this is the first study examining the association of LSFG metrics with theoretical predictions that are based on a multitude of vascular characteristics; hence, it allows for additional insight regarding properties and interpretation of LSFG outcomes. This is also the first study proposing such a multimodal approach for absolute, individualized predictions of vascular resistance and BF through simple clinical tests: fundus imaging, OCTA scans, BP and IOP measurements (or ophthalmodynamometry), and a blood sample.

With respect to physiology, this study implies that by assessing the phenotype of the perfused vasculature (extent of dilation/contraction, structural complexity, viscous forces, and perfusion pressure) at a specific timepoint, we are able to draw significant quantitative conclusions on its autoregulatory reserve, i.e., its ability to withstand transient BP drops or increases. Importantly, we used these findings to provide evidence that LARL in healthy subjects is closer to resting state than thought before; thus, big drops in perfusion pressure are not necessary for hypoperfusion to become relevant. It is noteworthy that such drops in perfusion pressure are not only linked to disease (e.g., glaucoma) but can also occur as episodes of orthostatic hypotension or nocturnal blood pressure dipping (see below). As already discussed, this implies that the retinal vasculature is better prepared to counteract transient rises rather than decreases in perfusion pressure.

Regarding clinical relevance, a recent study on diabetic retinopathy showed that a combination of fundus and OCTA measurements can already improve assessment of the disease (130). Another study used a fundus-based model to generate a fixed length feature vector as an index that can be used to successfully discriminate between healthy and glaucoma (96). However, since they used constant, nonindividualized inlet values and relied on the vessel structure to guide the outcome, the end point parameters are not easily interpretable. Our study showed that RBF predicted pRNFL thickness and GCC volume, and this effect was independent of age (Table 4). Therefore, aside from its potential merit in understanding pathophysiological mechanisms, the model possibly also offers useful clinical markers in diagnosing ocular pathologies.

In this regard, a low blood pressure (especially during the night), sometimes even when resulting from aggressive treatment of preexisting AHT (J-shape phenomenon), has been suggested as a risk factor for glaucoma development or progression in several studies (14, 79, 80, 85, 133, 150, 151). It is hypothesized that this association is mediated by hypoperfusion of the retinal ganglion cells, leading to their death; that said, since the retina exhibits AR properties, the subjects really at risk are probably the ones at the extremities of low BP or the ones with vascular dysregulation, that is, impaired AR (33, 49b). Notably, in all of the aforementioned studies regarding low BP and glaucoma, risk starts to increase around perfusion pressures comparable to LARL (37 mmHg with the classical definition). Our study suggests that subjects with low BP (or even with a BP ~1 SD lower than average, combined with an IOP ~1 SD higher than average) might already be below their LARL, suggesting these observations are of considerable clinical relevance. Importantly, a recent longitudinal study showed that the clinical entity of NTG (i.e., glaucomatous damage with IOP measured within the normal range) displayed faster progression in patients whose DBP dips low during the night (75). As previously mentioned, the fact that

LARL lies within the spectrum of values relevant to clinical management has already been suggested for the cerebral circulation (4, 23, 26, 29).

AHT has also been suggested itself as a risk factor for glaucoma, but a meta-analysis showed there exists significant heterogeneity across studies, sometimes even reporting protective associations (150). Increased glaucoma risk in patients with AHT could be, first of all, directly mediated by elevated IOP (54). In addition, both aggressive antihypertensive treatment (as previously mentioned) and poorly controlled, chronic AHT (resulting in endothelial damage, compromised AR, and disproportionately increased RVR) could also make certain subjects more susceptible to BF reduction, thus explaining this association (49b, 49c, 72). In this regard, our study estimated the lower perfusion pressure levels (43 mmHg with the classical OPP definition) that should be respected, to avoid overtreating AHT, especially in glaucoma patients or suspects. Regarding the protective associations between AHT and glaucoma that are sometimes reported, some studies provide evidence in favor of certain categories of antihypertensive medication with a potential neuroprotective effect (58, 59, 99, 145). Additionally, we hypothesize that well-controlled or newly established AHT could offer an initial protection to perfusion deficits, as has been observed in rodents (49a). Results from our study second that, since the AHT group had reduced susceptibility to IOP elevation, as far as perfusion is concerned (IOP = 26 mmHg was needed to bring the average subject with AHT to LARL, to be compared with IOP = 20 mmHg for the subjects without AHT).

Study Limitations

This study has several limitations. With regards to the model build, first, we did not obtain individualized information for Hct. Instead, we relied on reference values, adjusted for age, sex, and blood pressure status [see METHODS, *Model Variables and Parameters, Blood viscosity (μ)*]. Nevertheless, the sensitivity analysis (Table 3) revealed that Hct was still an important determinant of RVR and RBF, suggesting that analyzing blood samples in future studies might be a worthwhile consideration, with the potential to increase the accuracy of the model predictions.

Second, fractal dimension was considered as a global index, as measured from the SVP, inside a 3-mm-diameter circular ROI, centered at the fovea (see METHODS, *Model Variables and Parameters*, *Fractal dimension* and Fig. 1*B*). Therefore, it might ignore local variations attributed to anatomy or to disease-related focal microvascular dropout, outside the ROI (17, 93, 146). A more accurate representation of the vasculature would contribute to the understanding of crucial phenomena, such as localized flow deficits or tissue oxygen extraction and diffusion (36). However, adapting more heterogeneous or three-dimensional theoretical models to account for individualized estimations in the human eye would require further improvements in visualization and quantification of the interconnectivity between different capillary plexus. Again, the sensitivity analysis (Table 3) suggests that, even with this suboptimal calculation, fractal dimension slightly improves the model predictions.

Lastly, as already discussed, we only used approximations of the pressures in the CRA and CRV, based on the MAP and the IOP, respectively (see METHODS, *Model Variables and Parameters*, *Ocular perfusion pressure*); ophthalmodynamometric measurements could further refine the model predictions.

As far as the in vivo investigation limitations are concerned, we used a small sample size ($n = 36$) containing mostly healthy eyes. The small sample size does not provide optimal power for detecting low or medium effect sizes when fitting multivariable backward regression models (42). However, we made sure the saturated models contained only preselected variables, based on physiological expectations and previous literature reports. In addition, only a small number of variables with very strong associations ended up in the reduced models, while the effect size (R^2) was large; hence, our findings can be considered robust to this limitation. Notably, implementing forward regression with the same LSFG metrics yielded the exact same results.

According to the Windkessel effect, BF at any point throughout a cardiac cycle is the sum of resistive ("outlet") and capacitive ("storage") flow (35). Despite the fact that compliance is not expected to affect the mean blood flow estimate (i.e., RBF), as shown in APPENDIX D, our IOP stimulation poses some limitations, one of which is that it can only investigate static AR (114). Static AR describes the overall effect of the AR activity and is examined cross-sectionally before and after the stimulation. Notably, in dynamic AR (where the vascular response latency is also evaluated), compliance buffering has been shown to be more important than resistance changes in explaining blood velocity fluctuations, at least in cerebral vessels (134, 149). In addition, an experimental study revealed that chronic IOP elevation in glaucomatous eyes could also affect dynamic AR; therefore, considering solely static AR would likely underestimate the extent of hypoperfusion (138). This could enhance our findings, since it highlights the fact that the clinically relevant location of LARL can be even more alarming when we also consider potential defects in dynamic AR.

Conclusions

In summary, we used a novel approach to characterize two markers of the human retinal circulation (vascular resistance and blood flow), by combining standard clinical tests, quantitative static imaging techniques, and physiological modeling. We demonstrated that these predictions correlate strongly with dynamic blood flow metrics, as offered by laser speckle flowgraphy. We used these findings to generate autoregulation curves and estimated that the lower autoregulation limit is well inside the range of clinical significance, both in healthy subjects and in subjects receiving antihypertensive treatment. This suggests that autoregulatory mechanisms in the retina are more effective in counteracting increases, rather than decreases in perfusion pressure. Therefore, some retinas are more liable to hypoperfusion than previously thought, even after relatively small intraocular pressure rises or blood pressure drops. By using intraocular pressure stimulation, we showed that this lower autoregulation limit prediction was in agreement with in vivo physiological observations.

These findings could enhance our understanding of the vascular component in ophthalmic diseases and improve treatment decisions in patients with coexisting ophthalmic and cardiovascular pathology, especially arterial hypertension. In particular, monitoring retinal blood flow in longitudinal designs could elucidate the "chicken-egg" dilemma in glaucoma, according to which it is unknown whether reduced BF is the cause or consequence of RGC death. Further studies are needed to assess the diagnostic value of this approach, its efficacy in personalized

intervention, such as antihypertensive treatment, and its applicability in other vascular networks.

APPENDIX A

Calculation of RVR (Refer to METHODS, Model Building)

We first calculate the resistance of each vessel generation R_{a_i} in the arterial compartment, as a function of its radius. Similar reasoning applies to the venous compartment.

$$R_a(r) = \frac{R_b(r)}{N_b(r)} \tag{A1}$$

where $R_b(r)$ is the resistance of a single branch with radius r and $N_b(r)$ is the expected number of branches of radius r.

$R_b(r)$ can be calculated from Poiseuille's law and *Eqs. 2*, *3*, and *5* (main text). For an arteriole, it will be:

$$R_b(r) = \frac{8\mu(r)l(r)}{\pi r^4} = \ldots = \frac{8\mu_\infty \beta \left(\frac{\overline{r_{a_0}}}{r_{a_0}}\right)^\alpha}{\pi r^{2-\alpha}(r+\delta)^2} \tag{A2}$$

where $\delta = 4.29$ μm is the red-cell-size order of magnitude constant defined in *Eq. 5*.

$N_b(r)$ has been estimated by Kamiya and Takahashi (63). Again, for an arteriole:

$$N_b(r) = \left(\frac{r}{r_{a_0}}\right)^{-D-\alpha}. \tag{A3}$$

From *Eq. A3*, it is not difficult to show that, for symmetric and dichotomous branching, r_i is a geometric sequence. Hence:

$$r_i = \lambda^i r_0 \tag{A4}$$

where $\lambda = 2^{-\frac{1}{D+\alpha}}$ (which equals $e^{-\tau}$ as can be seen in *Eq. 1* of the main text) and, again, i is an integer representing the branch order.

The resistance of the capillaries R_c is constant:

$$R_c = \frac{8\mu_c l_c}{\pi r_c^4} 2^{-16} \tag{A5}$$

where we assume four branches per terminal arteriole/venule.

In the last step, we use *Eqs. A1–A5* to compute RVR:

$$\begin{aligned} \mathrm{RVR} &= \sum_{i=0}^{14} R_{a_i} + \sum_{j=0}^{14} R_{v_j} + R_c = \ldots \\ &= \frac{8\beta}{\pi}\left[\mu_{a_\infty} \frac{\overline{r_{a_0}}^\alpha}{r_{a_0}^2} \sum_{i=0}^{14} \frac{2^{\frac{D+2\alpha-2}{D+\alpha} i}}{\left(2^{-\frac{1}{D+\alpha} i} r_{a_0} + \delta\right)^2}\right. \\ &\left. + \mu_{v_\infty} \frac{\overline{r_{v_0}}^\alpha}{r_{v_0}^2} \sum_{j=0}^{14} \frac{2^{\frac{D+2\alpha-2}{D+\alpha} j}}{\left(2^{-\frac{1}{D+\alpha} j} r_{v_0} + \delta\right)^2}\right] + \frac{8\mu_c l_c}{\pi r_c^4} 2^{-16} \end{aligned} \tag{A6}$$

APPENDIX B

Flow Acceleration (Refer to DISCUSSION, Model Investigation Results, Laser Speckle Flowgraphy Metrics)

Let us consider a pressure difference $P(t)$ varying through the cardiac cycle as a single harmonic and accelerating blood of mass m inside a vessel of length l and radius r, with r large enough:

$$P(t) = M\cos(\omega t) + P_0, \quad t \in \left[0, \quad \frac{60}{\mathrm{HR}}\right] \tag{A7}$$

where M is the pulse amplitude, ω is the angular velocity ($2\pi \frac{\mathrm{HR}}{60}$), and P_0 is the average pressure difference. For the time-varying acceleration $\alpha(t)$, it follows that:

$$a(t) = \frac{[M\cos(\omega t) + P_0]\pi r^2}{m} = \frac{M\cos(\omega t) + P_0}{\varrho l} \tag{A8}$$

where ϱ is the blood density.

Therefore, FAI, which is the maximum acceleration during the systolic phase, in this case would largely depend on individual SBP values (central impulse) and would be independent from RVR (18):

$$FAI = a_{\max_{syst}} = \frac{M + P_0}{\varrho l} \tag{A9}$$

Due to the interdependence of *Eqs. 13* and *14* presented in the RESULTS and DISCUSSION, in Eq. A7, M can be considered a partial determinant of $u_{\max}$-$u_{\min}$, while P_0 can be seen as a partial determinant of $\bar{u}$. When adjusting for MV in the RVR regression model, the FAI-induced increase in RVR translates to increased PSV and decreased EDV.

APPENDIX C

Branching Optimization (Refer to DISCUSSION, Quantitative Vascular Analysis)

Consider a given (fixed) parent branch and let its two daughter branches (of unknown caliber) be two approximately parallel resistors R_S and R_L. Using *Eq. A2*, we introduce the following quantity:

$$\frac{1}{R_{\text{daughters}}} = \frac{1}{R_S} + \frac{1}{R_L} = K\left[r_S^{2-\alpha}(r_S+\delta)^2 + r_L^{2-\alpha}(r_L+\delta)^2\right] =$$

$$K\left[z_S^{\frac{2-\alpha}{D+\alpha}}\left(z_S^{\frac{1}{D+\alpha}} + \delta\right)^2 + z_L^{\frac{2-\alpha}{D+\alpha}}\left(z_L^{\frac{1}{D+\alpha}} + \delta\right)^2\right] \tag{A10}$$

where $z_S = r_S^{D+\alpha}$, $z_L = r_L^{D+\alpha}$ (with $z_S + z_L$ fixed according to *Eq. 17*), and K is a constant.

It can be shown that $f : [0, \quad +\infty) \to R$, defined as:

$$f(x) = Kx^{\frac{2-\alpha}{D+\alpha}}\left(x^{\frac{1}{D+\alpha}} + \delta\right)^2 \tag{A11}$$

is concave for all physiologically possible choices of D and α. Hence, from Jensen's inequality:

$$f(z_S) + f(z_L) \le 2f\left(\frac{z_S + z_L}{2}\right) \tag{A12}$$

where the left-hand side is precisely the quantity in *Eq. A10* and the right-hand side is a fixed number.

The upper bound in Jensen's inequality is attained if and only if $z_S = z_L$ (hence $r_S = r_L$) or f is linear; this equality case results in minimal total daughter resistance for a given parent branch (optimization principle). Upstream in the retinal circulation, perfectly symmetrical branching is not necessary for optimization: indeed, it can be shown that f is almost linear for large x (f " approaches zero). Toward the terminal vessels, f is more concave, hence symmetrical branching will favor BF optimization. Importantly, without the Fåhræus-Lindqvist effect (i.e., without δ in the equation), concavity of f is not guaranteed over all physiologically possible D and α (f would now become convex when $D + 2\alpha > 4$). Therefore, this particular optimization principle cannot be safely generalized to other fluids and branching structures.

APPENDIX D

Vascular Compliance (Refer to DISCUSSION, Study Limitations)

The simplest Windkessel equation (two-element) is displayed below:

$$Q(t) = \frac{P(t)}{\mathrm{RVR}} + CP'(t) = \frac{M\cos(\omega t) + P_0}{\mathrm{RVR}} - \omega C \sin(\omega t), \quad t \in \left[0, \frac{60}{\mathrm{HR}}\right] \tag{A13}$$

where we have kept the single-harmonic notation of *Eq. A7*, $Q(t)$ is the time-varying BF, and C is the vascular compliance (change in blood volume for a given change in perfusion pressure).

Clearly, since $\int_0^{2\pi} \cos x = \int_0^{2\pi} \sin x = 0$, compliance is not expected to affect the mean blood flow estimate (i.e., RBF), because *Eq. A13* reduces to *Eq. 8* (main text) when integrated over the complete Fourier series within one cardiac cycle.

ACKNOWLEDGMENTS

We thank Angela Ehmer (University Eye Clinic, Otto von Guericke University Magdeburg) for coordinating this study and contributing to the data collection.

GRANTS

This study was funded by the European Union's Horizon 2020 Research and Innovation Program under the Marie Sklodowska-Curie Grant Agreement No. 675033 European Glaucoma Research Training Program Plus (EGRET+).

DISCLAIMERS

The funding organization had no role in the design, conduct, analysis, or publication of this research.

DISCLOSURES

No conflicts of interest, financial or otherwise, are declared by the authors.

AUTHOR CONTRIBUTIONS

K.P., L.C. and N.J. conceived and designed research; K.P. and L.C. performed experiments; K.P. analyzed data; K.P., L.C. and N.J. interpreted results of experiments; K.P. prepared figures; K.P. drafted manuscript; K.P., L.C. and N.J. edited and revised manuscript; K.P., L.C. and N.J. approved final version of manuscript.

DATA AVAILABILITY

We declare that the raw data set and the image processing scripts are freely available upon request to the corresponding author [personalization of scripts is necessary to tailor the algorithms along noncompatible optical coherence tomography devices of different manufacturers] (https://doi.org/10.6084/m9.figshare.12982043.v1).

REFERENCES

1. **Akaishi T**, **Abe M**, **Miki T**, **Miki M**, **Funamizu Y**, **Ito S**, **Abe T**, **Ishii T.** Ratio of diastolic to systolic blood pressure represents renal resistive index. *J Hum Hypertens* 34: 512-519, 2020. doi:doi:10.1038/s41371-019-0264-1.
2. **Anonymous.** European Glaucoma Society Terminology and Guidelines for Glaucoma, 4th Edition - Chapter 3: Treatment principles and options Supported by the EGS Foundation: Part 1: Foreword; Introduction; Glossary; Chapter 3 Treatment principles and options. *Br J Ophthalmol* 101:130–195, 2017. doi:10.1136/bjophthalmol-2016-EGSguideline.003.
3. **Arciero J**, **Harris A**, **Siesky B**, **Amireskandari A**, **Gershuny V**, **Pickrell A**, **Guidoboni G.** Theoretical analysis of vascular regulatory mechanisms contributing to retinal blood flow autoregulation. *Invest Ophthalmol Vis Sci* 54: 5584–5593, 2013. doi:10.1167/iovs.12-11543.
4. **Armstead WM.** Cerebral blood flow autoregulation and dysautoregulation. *Anesthesiol Clin* 34: 465–477, 2016. doi:10.1016/j.anclin.2016.04.002.
5. **Aschinger GC**, **Schmetterer L**, **Fondi K**, **Aranha Dos Santos V**, **Seidel G**, **Garhöfer G**, **Werkmeister RM.** Effect of diffuse luminance flicker light stimulation on total retinal blood flow assessed with dual-beam bidirectional doppler OCT. *Invest Ophthalmol Vis Sci* 58: 1167–1178, 2017. doi:10.1167/iovs.16-20598.
6. **Attariwala R**, **Giebs CP**, **Glucksberg MR.** The influence of elevated intraocular pressure on vascular pressures in the cat retina. *Invest Ophthalmol Vis Sci* 35: 1019–1025, 1994.
7. **Attinger EO.** The physics of pulsatile blood flow with particular reference to small vessels. *Invest Ophthalmol* 4: 973–987, 1965.
8. **Bankhead P**, **Scholfield CN**, **McGeown JG**, **Curtis TM.** Fast retinal vessel detection and measurement using wavelets and edge location refinement. *PLoS One* 7: e32435, 2012. doi:10.1371/journal.pone.0032435.
9. **Bardelli M**, **Veglio F**, **Arosio E**, **Cataliotti A**, **Valvo E**, **Morganti A**; **Italian Group for the Study of Renovascular Hypertension.** New intrarenal echo-Doppler velocimetric indices for the diagnosis of renal artery stenosis. *Kidney Int* 69: 580–587, 2006. doi:10.1038/sj.ki.5000112.
10. **Barry DI.** Cerebral blood flow in hypertension. *J Cardiovasc Pharmacol* 7, *Suppl* 2: S94–S98, 1985. doi:10.1097/00005344-198507002-00018.
11. **Bhatti MS**, **Tang TB**, **Laude A.** Effects of water drinking test on ocular blood flow waveform parameters: a laser speckle flowgraphy study. *PLoS One* 12: e0181512, 2017. doi:10.1371/journal.pone.0181512.
12. **Binggeli T**, **Schoetzau A**, **Konieczka K.** In glaucoma patients, low blood pressure is accompanied by vascular dysregulation. *EPMA J* 9: 387–391, 2018. doi:10.1007/s13167-018-0155-5.
13. **Blanco PJ**, **Müller LO**, **Spence JD.** Blood pressure gradients in cerebral arteries: a clue to pathogenesis of cerebral small vessel disease. *Stroke Vasc Neurol* 2: 108–117, 2017. doi:10.1136/svn-2017-000087.
14. **Bowe A**, **Grünig M**, **Schubert J**, **Demir M**, **Hoffmann V**, **Kütting F**, **Pelc A**, **Steffen HM.** Circadian variation in arterial blood pressure and glaucomatous optic neuropathy–a systematic review and meta-analysis. *Am J Hypertens* 28: 1077–1082, 2015. doi:10.1093/ajh/hpv016.
15. **Brassard P**, **Ferland-Dutil H**, **Smirl JD**, **Paquette M**, **Le Blanc O**, **Malenfant S**, **Ainslie PN.** Evidence for hysteresis in the cerebral pressure-flow relationship in healthy men. *Am J Physiol Heart Circ Physiol* 312: H701–H704, 2017. doi:10.1152/ajpheart.00790.2016.
16. **Briers D**, **Duncan DD**, **Hirst E**, **Kirkpatrick SJ**, **Larsson M**, **Steenbergen W**, **Stromberg T**, **Thompson OB.** Laser speckle contrast imaging: theoretical and practical limitations. *J Biomed Opt* 18: 066018, 2013. doi:10.1117/1.JBO.18.6.066018.

16a. **Cabrera DeBuc D**, **Somfai GM**, **Koller A.** Retinal microvascular network alterations: potential biomarkers of cerebrovascular and neural diseases. *Am J Physiol Heart Circ Physiol* 312: H201–H212, 2017. doi:10.1152/ajpheart.00201.2016.

17. **Campbell JP**, **Zhang M**, **Hwang TS**, **Bailey ST**, **Wilson DJ**, **Jia Y**, **Huang D.** Detailed vascular anatomy of the human retina by projection-resolved optical coherence tomography angiography. *Sci Rep* 7: 42201, 2017. doi:10.1038/srep42201.
18. **Chemla D**, **Démolis P**, **Thyrault M**, **Annane D**, **Lecarpentier Y**, **Giudicelli JF.** Blood flow acceleration in the carotid and brachial arteries of healthy volunteers: respective contributions of cardiac performance and local resistance. *Fundam Clin Pharmacol* 10: 393–399, 1996. doi:10.1111/j.1472-8206.1996.tb00591.x.
19. **Cherecheanu AP**, **Garhofer G**, **Schmidl D**, **Werkmeister R**, **Schmetterer L.** Ocular perfusion pressure and ocular blood flow in glaucoma. *Curr Opin Pharmacol* 13: 36–42, 2013. doi:10.1016/j.coph.2012.09.003.
20. **Chien S**, **Usami S**, **Skalam R.** Blood flow in small tubes. In: Handbook of Physiology, edited by Renkin EM, Michel CC. Bethesda, MD: American Physiological Society, 1984, p. 217–249.
21. **Cirillo M**, **Laurenzi M**, **Trevisan M**, **Stamler J.** Hematocrit, blood pressure, and hypertension. The Gubbio Population Study. *Hypertension* 20: 319–326, 1992. doi:10.1161/01.HYP.20.3.319.
22. **Crutchfield KE**, **Razumovsky AY**, **Tegeler CH**, **Mozayeni BR.** Differentiating vascular pathophysiological states by objective analysis of flow dynamics. *J Neuroimaging* 14: 97–107, 2004. doi:10.1111/j.1552-6569.2004.tb00224.x.
23. **Czosnyka M**, **Miller C**; **Participants in the International Multidisciplinary Consensus Conference on Multimodality Monitoring.** Monitoring of cerebral autoregulation. *Neurocrit Care* 21, Suppl 2: S95–S102, 2014. doi:10.1007/s12028-014-0046-0.

24. **Dai C**, **Liu X**, **Zhang HF**, **Puliafito CA**, **Jiao S.** Absolute retinal blood flow measurement with a dual-beam Doppler optical coherence tomography. *Invest Ophthalmol Vis Sci* 54: 7998–8003, 2013. doi:10.1167/iovs.13-12318.
26. **Donnelly J**, **Czosnyka M**, **Adams H**, **Robba C**, **Steiner LA**, **Cardim D**, **Cabella B**, **Liu X**, **Ercole A**, **Hutchinson PJ**, **Menon DK**, **Aries MJ**, **Smielewski P.** Individualizing thresholds of cerebral perfusion pressure using estimated limits of autoregulation. *Crit Care Med* 45: 1464–1471, 2017. doi:10.1097/CCM.0000000000002575.
27. **Dorner GT**, **Polska E**, **Garhöfer G**, **Zawinka C**, **Frank B**, **Schmetterer L.** Calculation of the diameter of the central retinal artery from noninvasive measurements in humans. *Curr Eye Res* 25: 341–345, 2002. doi:10.1076/ceyr.25.6.341.14231.
28. **Draijer M**, **Hondebrink E**, **van Leeuwen T**, **Steenbergen W.** Review of laser speckle contrast techniques for visualizing tissue perfusion. *Lasers Med Sci* 24: 639–651, 2009. doi:10.1007/s10103-008-0626-3.
29. **Drummond JC.** The lower limit of autoregulation: time to revise our thinking? *Anesthesiology* 86: 1431–1433, 1997. doi:10.1097/00000542-199706000-00034.
30. **Fåhræus R**, **Lindqvist T.** The viscosity of the blood in narrow capillary tubes**.** *Am J Physiol Legacy Content* 96: 562–568, 1931.
31. **Feke GT**, **Tagawa H**, **Deupree DM**, **Goger DG**, **Sebag J**, **Weiter JJ.** Blood flow in the normal human retina. *Invest Ophthalmol Vis Sci* 30: 58–65, 1989.
32. **Flammer J**, **Konieczka K.** Retinal venous pressure: the role of endothelin. *EPMA J* 6: 21, 2015. doi:10.1186/s13167-015-0043-1.
33. **Flammer J**, **Konieczka K**, **Flammer AJ.** The primary vascular dysregulation syndrome: implications for eye diseases. *EPMA J* 4: 14, 2013. doi:10.1186/1878-5085-4-14.
34. **Flammer J**, **Orgül S**, **Costa VP**, **Orzalesi N**, **Krieglstein GK**, **Serra LM**, **Renard JP**, **Stefánsson E.** The impact of ocular blood flow in glaucoma. *Prog Retin Eye Res* 21: 359–393, 2002. doi:10.1016/S1350-9462(02)00008-3.
35. **Frank O.** The basic shape of the arterial pulse. First treatise: mathematical analysis. 1899. *J Mol Cell Cardiol* 22: 255–277, 1990. doi:10.1016/0022-2828(90)91460-O.
36. **Fry BC**, **Coburn EB**, **Whiteman S**, **Harris A**, **Siesky B**, **Arciero J.** Predicting retinal tissue oxygenation using an image-based theoretical model. *Math Biosci* 305: 1–9, 2018. doi:10.1016/j.mbs.2018.08.005.
37. **Fuchsjager-Mayrl G**, **Schmetterer L.** Characterization of retinal blood flow in healthy subjects (Abstract). *Acta Ophthalmol* 89, 2011.
38. **Ganesan P**, **He S**, **Xu H.** Analysis of retinal circulation using an image-based network model of retinal vasculature. *Microvasc Res* 80: 99–109, 2010. doi:10.1016/j.mvr.2010.02.005.
39. **Garcia JP Jr**, **Garcia PT**, **Rosen RB.** Retinal blood flow in the normal human eye using the canon laser blood flowmeter. *Ophthalmic Res* 34: 295–299, 2002. doi:10.1159/000065600.
40. **Gardiner SK**, **Cull G**, **Fortune B**, **Wang L.** Increased optic nerve head capillary blood flow in early primary open-angle glaucoma. *Invest Ophthalmol Vis Sci* 60: 3110–3118, 2019. doi:10.1167/iovs.19-27389.
41. **Garhofer G**, **Werkmeister R**, **Dragostinoff N**, **Schmetterer L.** Retinal blood flow in healthy young subjects. *Invest Ophthalmol Vis Sci* 53: 698–703, 2012. doi:10.1167/iovs.11-8624.
42. **Green SB.** How many subjects does it take to do a regression analysis. *Multivariate Behav Res* 26: 499–510, 1991. doi:10.1207/s15327906mbr2603_7.
43. **Guidoboni G**, **Harris A**, **Carichino L**, **Arieli Y**, **Siesky BA.** Effect of intraocular pressure on the hemodynamics of the central retinal artery: a mathematical model. *Math Biosci Eng* 11: 523–546, 2014. doi:10.3934/mbe.2014.11.523.
44. **Guidoboni G**, **Harris A**, **Cassani S**, **Arciero J**, **Siesky B**, **Amireskandari A**, **Tobe L**, **Egan P**, **Januleviciene I**, **Park J.** Intraocular pressure, blood pressure, and retinal blood flow autoregulation: a mathematical model to clarify their relationship and clinical relevance. *Invest Ophthalmol Vis Sci* 55: 4105–4118, 2014. doi:10.1167/iovs.13-13611.
45. **Guo S**, **Yin S**, **Tse G**, **Li G**, **Su L**, **Liu T.** Association between caliber of retinal vessels and cardiovascular disease: a systematic review and meta-analysis. *Curr Atheroscler Rep* 22: 16, 2020. doi:10.1007/s11883-020-0834-2.
46. **Hale JF**, **McDonald DA**, **Womersley JR.** Velocity profiles of oscillating arterial flow, with some calculations of viscous drag and the Reynolds numbers. *J Physiol* 128: 629–640, 1955. doi:10.1113/jphysiol.1955.sp005330.
47. **Halpern EJ**, **Merton DA**, **Forsberg F.** Effect of distal resistance on Doppler US flow patterns. *Radiology* 206: 761–766, 1998. doi:10.1148/radiology.206.3.9494498.
48. **Haynes RH.** Physical basis of the dependence of blood viscosity on tube radius. *Am J Physiol* 198: 1193–1200, 1960. doi:10.1152/ajplegacy.1960.198.6.1193.
49. **Hayreh SS.** Blood flow in the optic nerve head and factors that may influence it. *Prog Retin Eye Res* 20: 595–624, 2001. doi:10.1016/S1350-9462(01)00005-2.

49a. **He Z**, **Nguyen CT**, **Armitage JA**, **Vingrys AJ**, **Bui BV.** Blood pressure modifies retinal susceptibility to intraocular pressure elevation. *PLoS One* 7: e31104, 2012. doi:10.1371/journal.pone.0031104.

49b. **He Z**, **Vingrys AJ**, **Armitage JA**, **Bui BV.** The role of blood pressure in glaucoma. *Clin Exp Optom* 94: 133–149, 2011. doi:10.1111/j.1444-0938.2010.00564.x.

49c. **He Z**, **Vingrys AJ**, **Armitage JA**, **Nguyen CT**, **Bui BV.** Chronic hypertension increases susceptibility to acute IOP challenge in rats. *Invest Ophthalmol Vis Sci* 55: 7888–7895, 2014. doi:10.1167/iovs.14-15207.

50. **Heeman W**, **Steenbergen W**, **van Dam G**, **Boerma EC.** Clinical applications of laser speckle contrast imaging: a review. *J Biomed Opt* 24: 1–11, 2019. doi:10.1117/1.JBO.24.8.080901.
51. **Heine GH**, **Reichart B**, **Ulrich C**, **Köhler H**, **Girndt M.** Do ultrasound renal resistance indices reflect systemic rather than renal vascular damage in chronic kidney disease? *Nephrol Dial Transplant* 22: 163–170, 2007. doi:10.1093/ndt/gfl484.
52. **Heinze G**, **Wallisch C**, **Dunkler D.** Variable selection - a review and recommendations for the practicing statistician. *Biom J* 60: 431–449, 2018. doi:10.1002/bimj.201700067.
53. **Heitmar R**, **Kalitzeos AA**, **Panesar V.** Comparison of two formulas used to calculate summarized retinal vessel calibers. *Optom Vis Sci* 92: 1085–1091, 2015. doi:10.1097/OPX.0000000000000704.
54. **Hennis A**, **Wu SY**, **Nemesure B**, **Leske MC**; **Barbados Eye Studies Group.** Hypertension, diabetes, and longitudinal changes in intraocular pressure. *Ophthalmology* 110: 908–914, 2003. doi:10.1016/S0161-6420(03)00075-7.
58. **Hirooka K**, **Baba T**, **Fujimura T**, **Shiraga F.** Prevention of visual field defect progression with angiotensin-converting enzyme inhibitor in eyes with normal-tension glaucoma. *Am J Ophthalmol* 142: 523–525, 2006. doi:10.1016/j.ajo.2006.04.020.
59. **Horwitz A**, **Klemp M**, **Jeppesen J**, **Tsai JC**, **Torp-Pedersen C**, **Kolko M.** Antihypertensive medication postpones the onset of glaucoma: evidence from a nationwide study. *Hypertension* 69: 202–210, 2017. doi:10.1161/HYPERTENSIONAHA.116.08068.
60. **Iwase T**, **Akahori T**, **Yamamoto K**, **Ra E**, **Terasaki H.** Evaluation of optic nerve head blood flow in response to increase of intraocular pressure. *Sci Rep* 8: 17235, 2018. doi:10.1038/s41598-018-35683-y.
61. **Iwase T**, **Yamamoto K**, **Yanagida K**, **Ra E**, **Ito Y**, **Murotani K**, **Terasaki H.** Investigation of causes of sex-related differences in ocular blood flow in healthy eyes determined by laser speckle flowgraphy. *Sci Rep* 7: 13878, 2017. doi:10.1038/s41598-017-14118-0.
62. **Jia Y**, **Morrison JC**, **Tokayer J**, **Tan O**, **Lombardi L**, **Baumann B**, **Lu CD**, **Choi W**, **Fujimoto JG**, **Huang D.** Quantitative OCT angiography of optic nerve head blood flow. *Biomed Opt Express* 3: 3127–3137, 2012. doi:10.1364/BOE.3.003127.
63. **Kamiya A**, **Takahashi T.** Quantitative assessments of morphological and functional properties of biological trees based on their fractal nature. *J Appl Physiol (1985)* 102: 2315–2323, 2007. doi:10.1152/japplphysiol.00856.2006.
64. **Kannenkeril D**, **Harazny JM**, **Bosch A**, **Ott C**, **Michelson G**, **Schmieder RE**, **Friedrich S.** Retinal vascular resistance in arterial hypertension. *Blood Press* 27: 82–87, 2018. doi:10.1080/08037051.2017.1393311.
65. **Kawasaki R**, **Wang JJ**, **Rochtchina E**, **Lee AJ**, **Wong TY**, **Mitchell P.** Retinal vessel caliber is associated with the 10-year incidence of glaucoma: the Blue Mountains Eye Study. *Ophthalmology* 120: 84–90, 2013. doi:10.1016/j.ophtha.2012.07.007.
66. **Keane PA**, **Sadda SR.** Imaging chorioretinal vascular disease. *Eye (Lond)* 24: 422–427, 2010. doi:10.1038/eye.2009.309.
67. **Khawaja AP**, **Crabb DP**, **Jansonius NM.** The role of ocular perfusion pressure in glaucoma cannot be studied with multivariable regression analysis applied to surrogates. *Invest Ophthalmol Vis Sci* 54: 4619–4620, 2013. doi:10.1167/iovs.13-12487.

68. **Kim KE**, **Kim DM**, **Flammer J**, **Kim KN.** Central retinal venous pressure in eyes of normal-tension glaucoma patients with optic disc hemorrhage. *PLoS One* 10: e0127920, 2015. doi:10.1371/journal.pone.0127920.
69. **King LA**, **Stanton AV**, **Sever PS**, **Thom SA**, **Hughes AD.** Arteriolar length-diameter (L:D) ratio: a geometric parameter of the retinal vasculature diagnostic of hypertension. *J Hum Hypertens* 10: 417–418, 1996.
70. **Kiyota N**, **Shiga Y**, **Ichinohasama K**, **Yasuda M**, **Aizawa N**, **Omodaka K**, **Honda N**, **Kunikata H**, **Nakazawa T.** The impact of intraocular pressure elevation on optic nerve head and choroidal blood flow. *Invest Ophthalmol Vis Sci* 59: 3488–3496, 2018. doi:10.1167/iovs.18-23872.
71. **Knudtson MD**, **Lee KE**, **Hubbard LD**, **Wong TY**, **Klein R**, **Klein BE.** Revised formulas for summarizing retinal vessel diameters. *Curr Eye Res* 27: 143–149, 2003. doi:10.1076/ceyr.27.3.143.16049.
72. **van Koeverden AK**, **He Z**, **Nguyen CT**, **Vingrys AJ**, **Bui BV.** Systemic hypertension is not protective against chronic intraocular pressure elevation in a rodent model. *Sci Rep* 8: 7107, 2018. doi:10.1038/s41598-018-25264-4.
73. **Ku DN.** Blood flow in arteries. *Annu Rev Fluid Mech* 29: 399–434, 1997. doi:10.1146/annurev.fluid.29.1.399.
74. **Kur J**, **Newman EA**, **Chan-Ling T.** Cellular and physiological mechanisms underlying blood flow regulation in the retina and choroid in health and disease. *Prog Retin Eye Res* 31: 377–406, 2012. doi:10.1016/j.preteyeres.2012.04.004.
75. **Kwon J**, **Jo YH**, **Jeong D**, **Shon K**, **Kook MS.** Baseline systolic versus diastolic blood pressure dip and subsequent visual field progression in normal-tension glaucoma. *Ophthalmology* 126: 967–979, 2019. doi:10.1016/j.ophtha.2019.03.001.
76. **Lee B**, **Novais EA**, **Waheed NK**, **Adhi M**, **de Carlo TE**, **Cole ED**, **Moult EM**, **Choi W**, **Lane M**, **Baumal CR**, **Duker JS**, **Fujimoto JG.** En face Doppler optical coherence tomography measurement of total retinal blood flow in diabetic retinopathy and diabetic macular edema. *JAMA Ophthalmol* 135: 244–251, 2017. doi:10.1001/jamaophthalmol.2016.5774.
77. **Lehmann MV**, **Schmieder RE.** Remodeling of retinal small arteries in hypertension. *Am J Hypertens* 24: 1267–1273, 2011. doi:10.1038/ajh.2011.166.
78. **Leske MC.** Ocular perfusion pressure and glaucoma: clinical trial and epidemiologic findings. *Curr Opin Ophthalmol* 20: 73–78, 2009. doi:10.1097/ICU.0b013e32831eef82.
79. **Leske MC**, **Heijl A**, **Hyman L**, **Bengtsson B**, **Dong L**, **Yang Z**; **EMGT Group.** Predictors of long-term progression in the early manifest glaucoma trial. *Ophthalmology* 114: 1965–1972, 2007. doi:10.1016/j.ophtha.2007.03.016.
80. **Leske MC**, **Wu SY**, **Hennis A**, **Honkanen R**, **Nemesure B**; **BESs Study Group.** Risk factors for incident open-angle glaucoma: the Barbados Eye Studies. *Ophthalmology* 115: 85–93, 2008. doi:10.1016/j.ophtha.2007.03.017.
81. **Luft N**, **Wozniak PA**, **Aschinger GC**, **Fondi K**, **Bata AM**, **Werkmeister RM**, **Schmidl D**, **Witkowska KJ**, **Bolz M**, **Garhöfer G**, **Schmetterer L.** Ocular blood flow measurements in healthy white subjects using laser speckle flowgraphy. *PLoS One* 11: e0168190, 2016. doi:10.1371/journal.pone.0168190.
82. **Luft N**, **Wozniak PA**, **Aschinger GC**, **Fondi K**, **Bata AM**, **Werkmeister RM**, **Schmidl D**, **Witkowska KJ**, **Bolz M**, **Garhöfer G**, **Schmetterer L.** Measurements of retinal perfusion using laser speckle flowgraphy and doppler optical coherence tomography. *Invest Ophthalmol Vis Sci* 57: 5417–5425, 2016. doi:10.1167/iovs.16-19896.
83. **Malek J**, **Azar AT**, **Nasralli B**, **Tekari M**, **Kamoun H**, **Tourki R.** Computational analysis of blood flow in the retinal arteries and veins using fundus image. *Comput Math Appl* 69: 101–116, 2015. doi:10.1016/j.camwa.2014.11.017.
84. **McClatchey PM**, **Schafer M**, **Hunter KS**, **Reusch JE.** The endothelial glycocalyx promotes homogenous blood flow distribution within the microvasculature. *Am J Physiol Heart Circ Physiol* 311: H168–H176, 2016. doi:10.1152/ajpheart.00132.2016.
85. **Melgarejo JD**, **Lee JH**, **Petitto M**, **Yépez JB**, **Murati FA**, **Jin Z**, **Chávez CA**, **Pirela RV**, **Calmón GE**, **Lee W**, **Johnson MP**, **Mena LJ**, **Al-Aswad LA**, **Terwilliger JD**, **Allikmets R**, **Maestre GE**, **De Moraes CG.** Glaucomatous optic neuropathy associated with nocturnal dip in blood pressure: findings from the Maracaibo Aging Study. *Ophthalmology* 125: 807–814, 2018. doi:10.1016/j.ophtha.2017.11.029.
86. **Murray CD.** The physiological principle of minimum work: I. The vascular system and the cost of blood volume. *Proc Natl Acad Sci USA* 12: 207–214, 1926. doi:10.1073/pnas.12.3.207.
87. **Mursch-Edlmayr AS**, **Luft N**, **Podkowinski D**, **Ring M**, **Schmetterer L**, **Bolz M.** Laser speckle flowgraphy derived characteristics of optic nerve head perfusion in normal tension glaucoma and healthy individuals: a Pilot study. *Sci Rep* 8: 5343, 2018. doi:10.1038/s41598-018-23149-0.
88. **Mustur D**, **Vahedian Z**, **Bovet J**, **Mozaffarieh M.** Retinal venous pressure measurements in patients with Flammer syndrome and metabolic syndrome. *EPMA J* 8: 339–344, 2017. doi:10.1007/s13167-017-0105-7.
89. **Nagahara M**, **Tamaki Y**, **Tomidokoro A**, **Araie M.** In vivo measurement of blood velocity in human major retinal vessels using the laser speckle method. *Invest Ophthalmol Vis Sci* 52: 87–92, 2011. doi:10.1167/iovs.09-4422.
90. **Nagaoka T**, **Mori F**, **Yoshida A.** Retinal artery response to acute systemic blood pressure increase during cold pressor test in humans. *Invest Ophthalmol Vis Sci* 43: 1941–1945, 2002.
91. **Nagaoka T**, **Yoshida A.** Noninvasive evaluation of wall shear stress on retinal microcirculation in humans. *Invest Ophthalmol Vis Sci* 47: 1113–1119, 2006. doi:10.1167/iovs.05-0218.
92. **Nagel E**, **Vilser W.** Autoregulative behavior of retinal arteries and veins during changes of perfusion pressure: a clinical study. *Graefes Arch Clin Exp Ophthalmol* 242: 13–17, 2004. doi:10.1007/s00417-003-0663-3.
93. **Nesper PL**, **Fawzi AA.** Human parafoveal capillary vascular anatomy and connectivity revealed by optical coherence tomography angiography. *Invest Ophthalmol Vis Sci* 59: 3858–3867, 2018. doi:10.1167/iovs.18-24710.
94. **Omae T**, **Nagaoka T**, **Yoshida A.** Relationship between retinal blood flow and serum adiponectin concentrations in patients with type 2 diabetes mellitus. *Invest Ophthalmol Vis Sci* 56: 4143–4149, 2015. doi:10.1167/iovs.15-16447.
95. **O'Neill WC.** Renal resistive index: a case of mistaken identity. *Hypertension* 64: 915–917, 2014. doi:10.1161/HYPERTENSIONAHA.114.04183.
96. **Orlando JI**, **Breda JB**, **van Keer K**, **Blaschko MB**, **Blanco PJ Bulant CA.** Towards a glaucoma risk index based on simulated hemodynamics from fundus images. In: *Medical Image Computing and Computer Assisted Intervention*. Berlin, Germany: Springer, 2018, p. 65–73.
97. **Oshinski JN**, **Ku DN**, **Bohning DE**, **Pettigrew RI.** Effects of acceleration on the accuracy of MR phase velocity measurements. *J Magn Reson Imaging* 2: 665–670, 1992. doi:10.1002/jmri.1880020610.
98. **Pappelis K**, **Jansonius NM.** Quantification and repeatability of vessel density and flux as assessed by optical coherence tomography angiography. *Transl Vis Sci Technol* 8: 3, 2019. doi:10.1167/tvst.8.3.3.
99. **Pappelis K**, **Loiselle AR**, **Visser S**, **Jansonius NM.** Association of systemic medication exposure with glaucoma progression and glaucoma suspect conversion in the Groningen Longitudinal Glaucoma Study. *Invest Ophthalmol Vis Sci* 60: 4548–4555, 2019. doi:10.1167/iovs.19-27984.
100. **Patton N**, **Aslam T**, **Macgillivray T**, **Dhillon B**, **Constable I.** Asymmetry of retinal arteriolar branch widths at junctions affects ability of formulae to predict trunk arteriolar widths. *Invest Ophthalmol Vis Sci* 47: 1329–1333, 2006. doi:10.1167/iovs.05-1248.
101. **Pemp B**, **Cherecheanu AP**, **Garhofer G**, **Schmetterer L.** Calculation of central retinal artery diameters from non-invasive ocular haemodynamic measurements in type 1 diabetes patients. *Acta Ophthalmol* 91: e348–e352, 2013. doi:10.1111/aos.12069.
102. **Pires PW**, **Dams Ramos CM**, **Matin N**, **Dorrance AM.** The effects of hypertension on the cerebral circulation. *Am J Physiol Heart Circ Physiol* 304: H1598–H1614, 2013. doi:10.1152/ajpheart.00490.2012.
103. **Polska E**, **Kircher K**, **Ehrlich P**, **Vecsei PV**, **Schmetterer L.** RI in central retinal artery as assessed by CDI does not correspond to retinal vascular resistance. *Am J Physiol Heart Circ Physiol* 280: H1442–H1447, 2001. doi:10.1152/ajpheart.2001.280.4.H1442.
104. **Popel AS.** A model of pressure and flow distribution in branching networks. *J Appl Mech* 47: 247–253, 1980. doi:10.1115/1.3153650.
105. **Pournaras CJ**, **Rungger-Brändle E**, **Riva CE**, **Hardarson SH**, **Stefansson E.** Regulation of retinal blood flow in health and disease. *Prog Retin Eye Res* 27: 284–330, 2008. doi:10.1016/j.preteyeres.2008.02.002.
106. **Prada D**, **Harris A**, **Guidoboni G**, **Siesky B**, **Huang AM**, **Arciero J.** Autoregulation and neurovascular coupling in the optic nerve head. *Surv Ophthalmol* 61: 164–186, 2016. doi:10.1016/j.survophthal.2015.10.004.
107. **Pries AR**, **Secomb TW**, **Gaehtgens P**, **Gross JF.** Blood flow in microvascular networks. Experiments and simulation. *Circ Res* 67: 826–834, 1990. doi:10.1161/01.RES.67.4.826.
108. **Pries AR**, **Secomb TW**, **Gessner T**, **Sperandio MB**, **Gross JF**, **Gaehtgens P.** Resistance to blood flow in microvessels in vivo. *Circ Res* 75: 904–915, 1994. doi:10.1161/01.RES.75.5.904.

109. **Puchner S**, **Schmidl D**, **Ginner L**, **Augustin M**, **Leitgeb R**, **Szegedi S**, **Stjepanek K**, **Hommer N**, **Kallab M**, **Werkmeister RM**, **Schmetterer L**, **Garhofer G.** Changes in retinal blood flow in response to an experimental increase in IOP in healthy participants as assessed with Doppler optical coherence tomography. *Invest Ophthalmol Vis Sci* 61: 33, 2020. doi:10.1167/iovs.61.2.33.
110. **Riva CE**, **Grunwald JE**, **Petrig BL.** Autoregulation of human retinal blood flow. An investigation with laser Doppler velocimetry. *Invest Ophthalmol Vis Sci* 27: 1706–1712, 1986.
111. **Russell RW.** Evidence for autoregulation in human retinal circulation. *Lancet* 2: 1048–1050, 1973. doi:10.1016/S0140-6736(73)92658-5.
112. **Sainz A**, **Cabau J**, **Roberts VC.** Deceleration vs. acceleration: a haemodynamic parameter in the assessment of vascular reactivity. A preliminary study. *Med Eng Phys* 17: 91–95, 1995. doi:10.1016/1350-4533(95)91878-K.
113. **Saltelli A**, **Andres TH**, **Homma T.** Sensitivity analysis of model output. *Comput Stat Data Anal* 15: 211–238, 1993. doi:10.1016/0167-9473(93)90193-W.
114. **Schmidl D**, **Garhofer G**, **Schmetterer L.** The complex interaction between ocular perfusion pressure and ocular blood flow - relevance for glaucoma. *Exp Eye Res* 93: 141–155, 2011. doi:10.1016/j.exer.2010.09.002.
115. **Secomb TW.** Hemodynamics. *Compr Physiol* 6: 975–1003, 2016. doi:10.1002/cphy.c150038.
116. **Shiga Y**, **Omodaka K**, **Kunikata H**, **Ryu M**, **Yokoyama Y**, **Tsuda S**, **Asano T**, **Maekawa S**, **Maruyama K**, **Nakazawa T.** Waveform analysis of ocular blood flow and the early detection of normal tension glaucoma. *Invest Ophthalmol Vis Sci* 54: 7699–7706, 2013. doi:10.1167/iovs.13-12930.
117. **Skalak R**, **Ozkaya N**, **Skalak TC.** Biofluid mechanics. *Annu Rev Fluid Mech* 21: 167–200, 1989. doi:10.1146/annurev.fl.21.010189.001123.
118. **Spaide RF**, **Fujimoto JG**, **Waheed NK**, **Sadda SR**, **Staurenghi G.** Optical coherence tomography angiography. *Prog Retin Eye Res* 64: 1–55, 2018. doi:10.1016/j.preteyeres.2017.11.003.
119. **Srinivas S**, **Tan O**, **Wu S**, **Nittala MG**, **Huang D**, **Varma R**, **Sadda SR.** Measurement of retinal blood flow in normal Chinese-American subjects by Doppler Fourier-domain optical coherence tomography. *Invest Ophthalmol Vis Sci* 56: 1569–1574, 2015. doi:10.1167/iovs.14-15038.
120. **Stodtmeister R**, **Oppitz T**, **Spoerl E**, **Haustein M**, **Boehm AG.** Contact lens dynamometry: the influence of age. *Invest Ophthalmol Vis Sci* 51: 6620–6624, 2010. doi:10.1167/iovs.09-4594.
121. **Stodtmeister R**, **Ventzke S**, **Spoerl E**, **Boehm AG**, **Terai N**, **Haustein M**, **Pillunat LE.** Enhanced pressure in the central retinal vein decreases the perfusion pressure in the prelaminar region of the optic nerve head. *Invest Ophthalmol Vis Sci* 54: 4698–4704, 2013. doi:10.1167/iovs.12-10607.
122. **Stoner L**, **McCully KK.** Velocity acceleration as a determinant of flow-mediated dilation. *Ultrasound Med Biol* 38: 580–592, 2012. doi:10.1016/j.ultrasmedbio.2011.12.024.
123. **Stoner L**, **Young JM**, **Fryer S**, **Sabatier MJ.** The importance of velocity acceleration to flow-mediated dilation. *Int J Vasc Med* 2012: 589213, 2012. doi:10.1155/2012/589213.
124. **Sugiyama T.** Basic technology and clinical applications of the updated model of laser speckle flowgraphy to ocular diseases. *Photonics* 1: 220–234, 2014. doi:10.3390/photonics1030220.
125. **Sung CK**, **Lee KH**, **Kim SH.** Evaluation of factors influencing arterial Doppler waveforms in an *in vitro* flow phantom. *Ultrasonography* 36: 39–52, 2017. doi:10.14366/usg.15055.
126. **Susanna R Jr**, **Hatanaka M**, **Vessani RM**, **Pinheiro A**, **Morita C.** Correlation of asymmetric glaucomatous visual field damage and water-drinking test response. *Invest Ophthalmol Vis Sci* 47: 641–644, 2006. doi:10.1167/iovs.04-0268.
127. **Szegedi S**, **Hommer N**, **Kallab M**, **Puchner S**, **Schmidl D**, **Werkmeister RM**, **Garhöfer G**, **Schmetterer L.** Repeatability and reproducibility of total retinal blood flow measurements using bi-directional Doppler OCT. *Transl Vis Sci Technol* 9: 34, 2020. doi:10.1167/tvst.9.7.34.
128. **Takahashi T**, **Nagaoka T**, **Yanagida H**, **Saitoh T**, **Kamiya A**, **Hein T**, **Kuo L**, **Yoshida A.** A mathematical model for the distribution of hemodynamic parameters in the human retinal microvascular network. *J Biorheol* 23: 77–86, 2009. doi:10.1007/s12573-009-0012-1.
129. **Tamaki Y**, **Araie M**, **Kawamoto E**, **Eguchi S**, **Fujii H.** Noncontact, two-dimensional measurement of retinal microcirculation using laser speckle phenomenon. *Invest Ophthalmol Vis Sci* 35: 3825–3834, 1994.
130. **Tan TE**, **Nguyen Q**, **Chua J**, **Schmetterer L**, **Tan GS**, **Wong CW**, **Tsai A**, **Cheung GC**, **Wong TY**, **Ting DS.** Global assessment of retinal arteriolar, venular and capillary microcirculations using fundus photographs and optical coherence tomography angiography in diabetic retinopathy. *Sci Rep* 9: 11751, 2019. doi:10.1038/s41598-019-47770-9.
131. **Tani T**, **Nagaoka T**, **Nakabayashi S**, **Yoshioka T**, **Yoshida A.** Autoregulation of retinal blood flow in response to decreased ocular perfusion pressure in cats: comparison of the effects of increased intraocular pressure and systemic hypotension. *Invest Ophthalmol Vis Sci* 55: 360–367, 2014. doi:10.1167/iovs.13-12591.
132. **Thom S.** Arterial structural modifications in hypertension. Effects of treatment. *Eur Heart J* 18, Suppl E: E2–E4, 1997. doi:10.1016/S0195-668X(97)90001-4.
133. **Topouzis F**, **Wilson MR**, **Harris A**, **Founti P**, **Yu F**, **Anastasopoulos E**, **Pappas T**, **Koskosas A**, **Salonikiou A**, **Coleman AL.** Association of open-angle glaucoma with perfusion pressure status in the Thessaloniki Eye Study. *Am J Ophthalmol* 155: 843–851, 2013. doi:10.1016/j.ajo.2012.12.007.
134. **Tzeng YC**, **Chan GS**, **Willie CK**, **Ainslie PN.** Determinants of human cerebral pressure-flow velocity relationships: new insights from vascular modelling and Ca^{2+} channel blockade. *J Physiol* 589: 3263–3274, 2011. doi:10.1113/jphysiol.2011.206953.
135. **Ulrich WD.** *Grundlagen und Methodik der Ophthalmodynamometrie (ODM), Ophthalmodynamographie (ODG), Temporalisdynamographie (TDG).* Leipzig, Germany: VEB Georg Thieme, 1976.
136. **Vosborg F**, **Malmqvist L**, **Hamann S.** Non-invasive measurement techniques for quantitative assessment of optic nerve head blood flow. *Eur J Ophthalmol* 30: 235–244, 2019. doi:10.1177/1120672119858891.
137. **Wang L**, **Cull GA**, **Fortune B.** Optic nerve head blood flow response to reduced ocular perfusion pressure by alteration of either the blood pressure or intraocular pressure. *Curr Eye Res* 40: 359–367, 2015. doi:10.3109/02713683.2014.924146.
138. **Wang L**, **Cull G**, **Burgoyne CF**, **Thompson S**, **Fortune B.** Longitudinal alterations in the dynamic autoregulation of optic nerve head blood flow revealed in experimental glaucoma. *Invest Ophthalmol Vis Sci* 55: 3509–3516, 2014. doi:10.1167/iovs.14-14020.
139. **Wang Y**, **Fawzi AA**, **Tan O**, **Zhang X**, **Huang D.** Flicker-induced changes in retinal blood flow assessed by Doppler optical coherence tomography. *Biomed Opt Express* 2: 1852–1860, 2011. doi:10.1364/BOE.2.001852.
140. **Vander Werff TJ.** The pressure measured in ophthalmodynamometry. *Arch Ophthalmol* 87: 290–292, 1972. doi:10.1001/archopht.1972.01000020292011.
141. **Werkmeister RM**, **Schmidl D**, **Aschinger G**, **Doblhoff-Dier V**, **Palkovits S**, **Wirth M**, **Garhöfer G**, **Linsenmeier RA**, **Leitgeb RA**, **Schmetterer L.** Retinal oxygen extraction in humans. *Sci Rep* 5: 15763, 2015. doi:10.1038/srep15763.
142. **Williams B**, **Mancia G**, **Spiering W**, **Rosei EA**, **Azizi M**, **Burnier M**, **Clement DL**, **Coca A**, **de Simone G**, **Dominiczak A**, **Kahan T**, **Mahfoud F**, **Redon J**, **Ruilope L**, **Zanchetti A**, **Kerins M**, **Kjeldsen SE**, **Kreutz R**, **Laurent S**, **Lip GY**, **McManus R**, **Narkiewicz K**, **Ruschitzka F**, **Schmieder RE**, **Shlyakhto E**, **Tsioufis C**, **Aboyans V**, **Desormais I.** [2018 ESC/ESH Guidelines for the management of arterial hypertension. The Task Force for the management of arterial hypertension of the European Society of Cardiology (ESC) and the European Society of Hypertension (ESH)]. *G Ital Cardiol (Rome)* 19: 3–73, 2018.
143. **Witkowska KJ**, **Bata AM**, **Calzetti G**, **Luft N**, **Fondi K**, **Wozniak PA**, **Schmidl D**, **Bolz M**, **Popa-Cherecheanu A**, **Werkmeister RM**, **Garhöfer G**, **Schmetterer L.** Optic nerve head and retinal blood flow regulation during isometric exercise as assessed with laser speckle flowgraphy. *PLoS One* 12: e0184772, 2017. doi:10.1371/journal.pone.0184772.
144. **Womersley JR.** Method for the calculation of velocity, rate of flow and viscous drag in arteries when the pressure gradient is known. *J Physiol* 127: 553–563, 1955. doi:10.1113/jphysiol.1955.sp005276.
145. **Yang H**, **Hirooka K**, **Fukuda K**, **Shiraga F.** Neuroprotective effects of angiotensin II type 1 receptor blocker in a rat model of chronic glaucoma. *Invest Ophthalmol Vis Sci* 50: 5800–5804, 2009. doi:10.1167/iovs.09-3678.
146. **Yarmohammadi A**, **Zangwill LM**, **Diniz-Filho A**, **Suh MH**, **Manalastas PI**, **Fatehee N**, **Yousefi S**, **Belghith A**, **Saunders LJ**, **Medeiros FA**, **Huang D**, **Weinreb RN.** Optical coherence tomography angiography vessel density in healthy, glaucoma suspect, and glaucoma eyes. *Invest Ophthalmol Vis Sci* 57: OCT451–OCT459, 2016. doi:10.1167/iovs.15-18944.

147. **Yip W**, **Tham YC**, **Hsu W**, **Lee ML**, **Klein R**, **Klein B**, **Ikram MK**, **Wong TY**, **Cheung CY.** Comparison of common retinal vessel caliber measurement software and a conversion algorithm. *Transl Vis Sci Technol* 5: 11, 2016. doi:10.1167/tvst.5.5.11.
148. **Yoo E**, **Yoo C**, **Lee BR**, **Lee TE**, **Kim YY.** Diagnostic ability of retinal vessel diameter measurements in open-angle glaucoma. *Invest Ophthalmol Vis Sci* 56: 7915–7922, 2015. doi:10.1167/iovs.15-18087.
149. **Zhang R**, **Behbehani K**, **Levine BD.** Dynamic pressure-flow relationship of the cerebral circulation during acute increase in arterial pressure. *J Physiol* 587: 2567–2577, 2009. doi:10.1113/jphysiol.2008.168302.
150. **Zhao D**, **Cho J**, **Kim MH**, **Guallar E.** The association of blood pressure and primary open-angle glaucoma: a meta-analysis. *Am J Ophthalmol* 158: 615–627, 2014. doi:10.1016/j.ajo.2014.05.029.
151. **Zheng Y**, **Wong TY**, **Mitchell P**, **Friedman DS**, **He M**, **Aung T.** Distribution of ocular perfusion pressure and its relationship with open-angle glaucoma: the Singapore Malay Eye Study. *Invest Ophthalmol Vis Sci* 51: 3399–3404, 2010. doi:10.1167/iovs.09-4867.